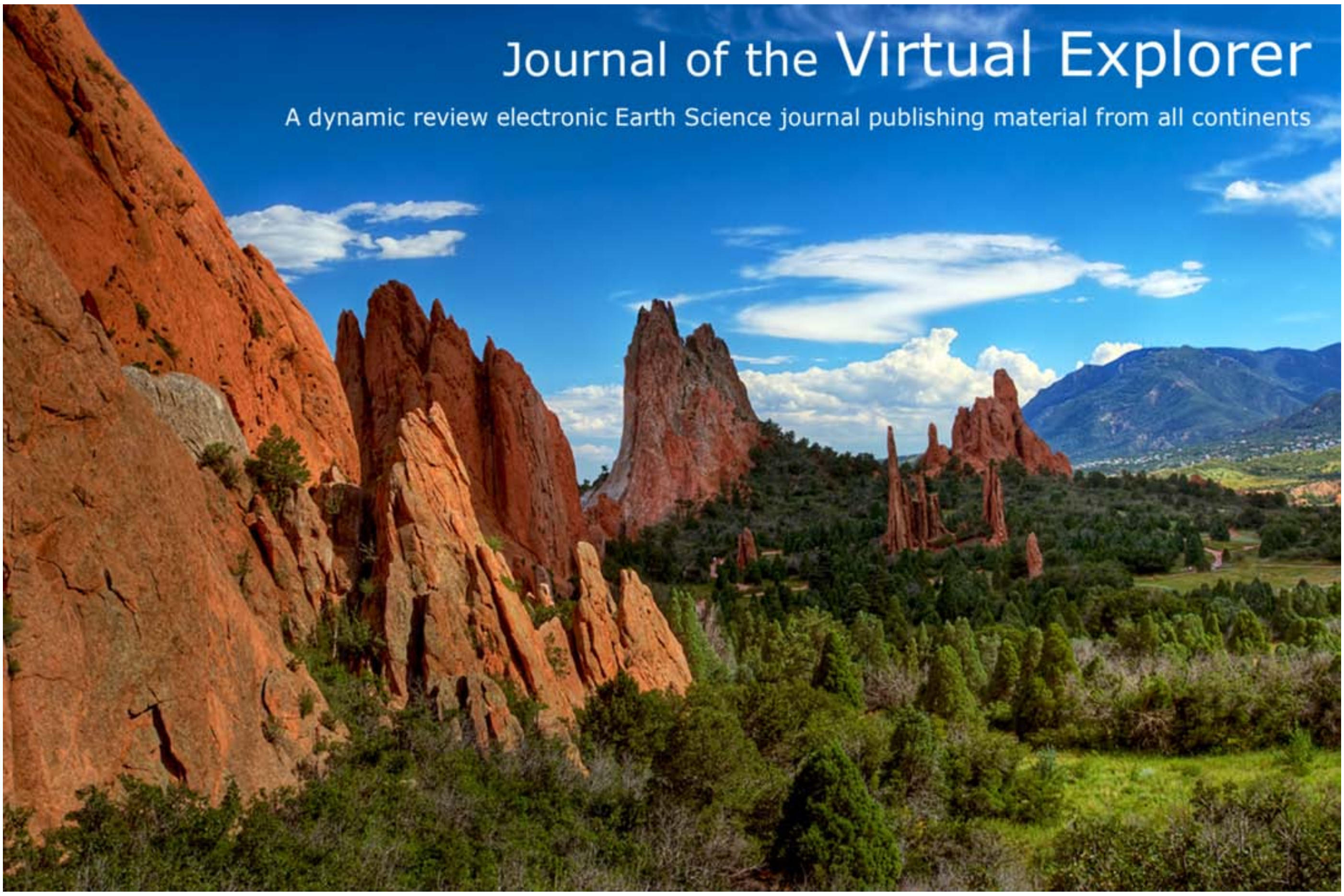

From tonalite to mylonite: coupled mechanical and chemical processes in foliation development and strain localization

Scott E. Johnson, Jeffrey H. Marsh, Ron H. Vernon

Journal of the Virtual Explorer, Electronic Edition, ISSN 1441-8142, volume 30, paper 5
In: (Ed.) Declan De Paor, Making Sense of Shear (In honour of Carol Simpson), 2008.

From tonalite to mylonite: coupled mechanical and chemical processes in foliation development and strain localization

Scott E. Johnson, Jeffrey H. Marsh, Ron H. Vernon

Journal of the Virtual Explorer, Electronic Edition, ISSN 1441-8142, volume **30**, paper 5
In: (Ed.) Declan De Paor, Making Sense of Shear (In honour of Carol Simpson), 2008.

Abstract: Microstructural and chemical processes interacted in the transformation of a hornblende-biotite tonalite to a mylonite in an approximately 28-m wide shear zone on the margins of the Cerro de Costilla complex, Baja California, México. Deformation in the tonalite at the edge of the shear zone was initiated by cleavage slip in biotite, leading to wispy, discontinuous foliae. Fracturing of the load-supporting plagioclase framework occurred at the edges and tips of biotite grains. With increasing strain, these foliae became linked via fine-grained aggregates involving fragmental and recrystallized biotite, recrystallized quartz, fragmental plagioclase, minor recrystallized myrmekite, and minor fragmental hornblende, titanite and epidote.

The amount of strain accumulation increases markedly across a sharp reaction front approximately 1 m from wall-rock orthogneisses. The front is characterized by metasomatic alteration, which resulted in the disappearance of hornblende in favor of biotite and quartz. Stronger deformation resulted in biotite-quartz-plagioclase 'beards' behind resistant plagioclase clasts. In the most highly strained tonalite, overall grainsize reduction was accompanied by a steady decrease in modal plagioclase, and increases in modal biotite and quartz.

Weakening and strain localization were accommodated by: (1) breakdown of the load-bearing plagioclase framework; (2) development of continuous biotite-rich foliae; (3) flow of quartz into lenticular foliae; (4) elimination of strong hornblende, accompanied by modal increase of weaker biotite; (5) dissolution, transport and re-deposition of biotite and quartz components in lower shear-strain sites; and (6) minor contributions from fine-grained aggregates of other minerals. These

http://virtualexplorer.com.au/article/2009/208/from-tonalite-to-mylonite

Citation: Johnson, S., Marsh, J., Vernon, R. 2008. From tonalite to mylonite: coupled mechanical and chemical processes in foliation development and strain localization. In: (Ed.) Declan De Paor, *Journal of the Virtual Explorer*, volume **30**, paper 5, doi: 10.3809/jvirtex.2009.00208

1. Introduction

The aim of this investigation is to evaluate the mechanical and chemical processes involved in the initiation and development of a mylonitic foliation in hornblende-biotite tonalite of the Cerro de Costilla complex, Baja California, México (Fig. 1). Many studies have shown that the development of a mylonitic foliation is accompanied by moderate to extreme grainsize reduction. Most of these studies have attempted to trace the progression from protomylonites with relatively large amounts of strain to mylonites or ultramylonites. This study explores the breakdown of a relatively homogeneous, undeformed protolith to a mylonite in which the phyllosilicates form an interconnected network of low-stress microshear zones. Stages of progressive fabric development are preserved across an approximately 28-m wide strain gradient at the margin of the complex, from essentially undeformed, coarse-grained tonalite to fine-grained, foliated mylonite at the wall-rock contact. We describe microstructural details of the transition, in which the interconnectivity of biotite and consequent foliation development were facilitated by fracture-assisted breakdown of a strong plagioclase framework, in addition to metasomatically-induced mineralogical changes. Whole-rock and mineral chemical data suggest a fluid infiltration front in the highest-strain rocks within 1 m of the host-rock contact, and we discuss the role of this inferred fluid in reactions that led to a modal increase in relatively weak minerals, namely biotite and quartz.

Figure 1. Geologic map showing the location of the Cerro de Costilla complex.

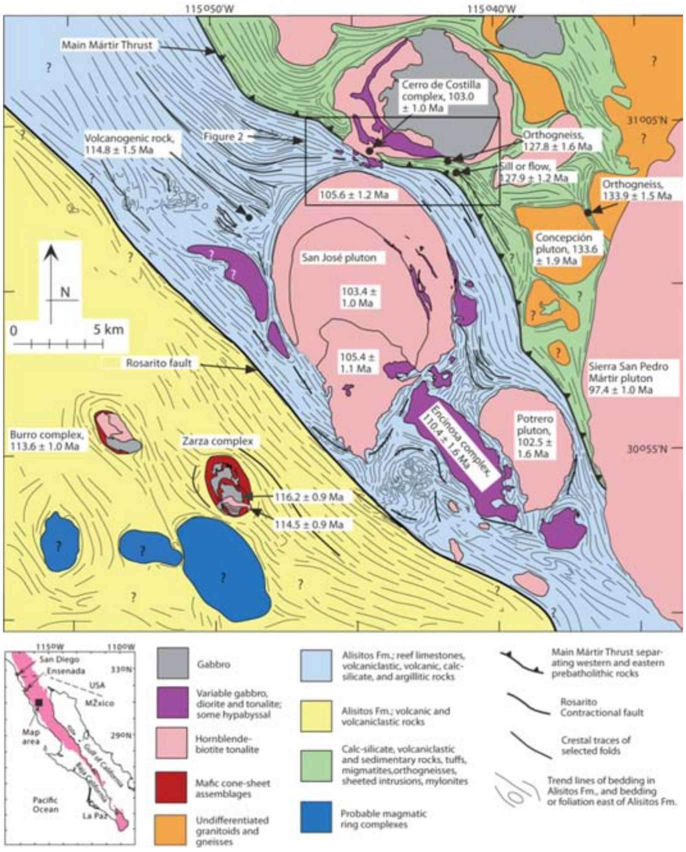

Geologic map of the San Jose pluton and surrounding region, from Johnson et al. (2003) with modifications from Melis (2006). The Cerro de Costilla complex is located in upper-center of the map. One age from the southern part of the complex is shown. All ages are from SHRIMP U-Pb zircon data reported in Johnson *et al.* (1999, 2003). See legend for geological information. Inset map at lower left shows the Baja California peninsula; the Peninsular Ranges batholith and adjacent pre-batholithic country rocks are shaded.

Grainsize reduction can arise from both brittle and ductile processes (e.g., Bell and Etheridge, 1973; White *et al.*, 1980; Vernon *et al.*, 1983; Segall and Simpson, 1986; Tullis and Yund, 1987; Goodwin and Wenk, 1995; Vernon *et al.*, 2004; Ree *et al.*, 2005), and is generally considered to be an important cause of strain localization in shear zones (e.g., White, 1979; Handy, 1989; Drury *et al.*, 1991; Jin *et al.*, 1998; Montesi and Hirth, 2003; Ree *et al.*, 2005; Oesterling *et al.*, 2007). In polymineralic rocks, an equally important mechanism for localization involves the interconnection of originally dispersed weak minerals, such as phyllosilicates (e.g., Kronenberg *et al.*, 1990; Shea and Kronenberg, 1992, 1993; Mares and Kronenberg, 1993; Wintsch *et al.*, 1995; Bos & Spiers, 2001;

Johnson *et al.*, 2004; Vernon *et al.*, 2004; Neimeijer and Spiers, 2005; Holyoke & Tullis, 2006; Mariani *et al.*, 2006; Marsh *et al.*, in press). Coalescence of weak minerals into interconnected, anastomosing networks facilitates weakening, and may be particularly important at crustal levels coincident with the frictional-to-viscous transition (Wintsch *et al.*, 1995; Stewart *et al.*, 2000; Imber *et al.*, 2001; Faulkner *et al.*, 2003; Collettini and Holdsworth, 2004; Mariani *et al.*, 2006; Marsh *et al.*, in press), where mylonitic shear zones represent the roots of major faults and control the coupling of deformation between the middle and upper crust (e.g., Handy *et al.*, 2007).

Theoretical and experimental work has shown that the bulk rheology of polymineralic rocks is dominated by the weakest mineral at volume fractions as low as approximately 15% (*e.g.*, Price, 1982; Tharp, 1983; Jordan, 1987, 1988; Ross *et al.*, 1987; Handy, 1990, 1994; Bons and Urai, 1994; Bons and Cox, 1994; Handy *et al.*, 1999; Johnson *et al.*, 2004; Holyoke & Tullis, 2006). However, the volume fraction of weak minerals, particularly phyllosilicates, commonly increases with increasing strain in shear zones, owing to syndeformational metamorphic hydration reactions (*e.g.*, Vernon *et al.*, 1983, Fitzgerald and Stunitz, 1993, Wintsch *et al.*, 1995, Yonkee *et al.*, 2003; Marsh *et al.*, in press). Consequently, coupling of mechanical and chemical processes can lead to extreme weakening, which results in increased strain rates, additional grainsize reduction and enhanced reaction rates.

The mechanism of weak-phase linkage is typically difficult to identify in naturally deformed rocks, because the process initiates at extremely low strains, and the evidence is typically obliterated by progressive deformation and recrystallization/neocrystallization (*e.g.*, Christiansen and Pollard, 1997; Bons and Jessell, 1999; Handy *et al.*, 2001; Johnson *et al.*, 2004). To find such evidence in polymineralic rocks, it is necessary to examine complete strain gradients. In addition, owing to the control exerted by preexisting layering, such as bedding or tectonic foliation, it is advantageous to study discrete shear zones in coarse-grained, non-foliated igneous rocks containing dispersed weak and strong minerals. Several studies have examined strain and fabric gradients in deformed granitoids involving strain-dependent coalescence of mica (*e.g.*, Berthé *et al.*, 1979; Simpson, 1985, 1985; Gapais, 1989; Lonka *et al.*, 1998; Vernon *et al.*, 2004; Johnson *et al.*, 2004; Marsh *et al.*, in press).

The two-part study of Vernon *et al.* (2004) and Johnson *et al.* (2004) is unusual, in that evidence for the microstructural mechanisms responsible for coalescence of originally dispersed biotite grains is clearly preserved. These authors found that linkage was initiated in undeformed tonalite by fracturing of the load-bearing plagioclase framework between intervening biotite grains, the fractures typically emanating from the tips of biotite grains, parallel to their (001) crystallographic faces. This was attributed to instantaneous strain-rate gradients among the different minerals (Johnson *et al.*, 2004), as also argued by Tullis *et al.* (1991). Johnson *et al.* (2004) conducted numerical experiments to investigate foliation initiation, reporting a stress and strain-rate evolution strikingly similar to that found in later laboratory experiments on fine-grained biotite gneiss (Holyoke and Tullis, 2006). A similar process was identified in calcite-halite experiments (Jordan, 1987) and in low-temperature experiments on mica schists (Gottschalk *et al.*, 1990; Shea and Kronenberg, 1992, 1993; Rawling *et al.*, 2002).

The deformation gradient studied by Vernon *et al.* (2004) and Johnson *et al.* (2004) is not easily related to deformation experiments, because the rocks show evidence for the presence of a small amount of partial melt during the deformation. Thus, it is unclear what role fluid-enhanced embrittlement (*e.g.*, Davidson *et al.*, 1994; Connolly *et al.*, 1997; Holyoke and Rushmer, 2002) may have played in fracturing and initiation of microshear zones. Therefore, one of our purposes here is to carefully examine the microstructural evidence for initiation of weak-phase linkages in a tonalite that shows no microstructural evidence that melt was present during the deformation, but instead reflects the results of brittle and crystal-plastic, solid-state processes, coupled with chemical reactions and metasomatic changes. The tonalite studied here is compositionally and modally nearly identical to the San José tonalite studied by Vernon *et al.* (2004) and Johnson *et al.* (2004). The deformation gradient in the San José tonalite was considered by these authors and Johnson *et al.* (2003) to have formed at high strain rates during emplacement and cooling of the magma. In contrast, the strain gradient evaluated here formed during greenschist-facies regional deformation. These two examples provide evidence for how strain localizes at different conditions, but for both, a key feature is coalescence of originally dispersed biotite grains into anastomosing microshear zones.

2. Geological setting

The 80 km^2 Cerro de Costilla complex (Fig. 1) is located in the Sierra San Pedro Mártir region of the Jurassic to Cretaceous Peninsular Ranges batholith in northern Baja California, México (*e.g.* Gastil *et al.*, 1975; Johnson *et al.*, 1999, 2003; Melis, 2006). From margins to core, the complex consists of (1) a nearly complete outer ring of tonalite, (2) a partial ring of deformed and partially melted metasedimentary and meta-igneous rocks, with zones of variably mingled gabbro, diorite and tonalite, (3) a partial inner ring of tonalite, and (4) a core of coarse-grained gabbro. On the basis of its distinctive geometry, Johnson *et al.* (2002) described the Cerro de Costilla as a magmatic ring complex, a conclusion supported by more extensive mapping (Melis, 2006). The mylonitic transition described here occurs in the outer tonalite ring; so the following discussion will focus on that unit.

The outer ring is composed of coarse-grained hornblende-biotite tonalite with abundant (~1%) microgranitoid enclaves. Johnson *et al.* (1999, 2003) reported a SHRIMP U/Pb age for the tonalite of 103 ± 1.0 Ma. The pluton was emplaced at pressures of 3-4 kbar (Melis, 2006, unpublished Al-in-hornblende data). The tonalite and the rest of the magmatic complex show a variably-developed magmatic foliation defined by alignment of plagioclase, hornblende and biotite grains. The tonalite cuts migmatitic gneisses in the hanging wall of the Main Martir Thrust, and so provides a younger limit to the relative age of the main movement on the thrust (Johnson *et al.*, 1999). During thrusting, a prominent north- to northeast-dipping foliation developed in both the hanging wall and footwall rocks. In the hanging wall, this foliation development was accompanied by partial melting, evidence of which is preserved as migmatite. A later tectonic foliation locally cuts the hanging wall rocks immediately to the south and southeast of the Cerro de Costilla complex. It is a steeply north- to northeast-dipping S/C fabric (Simpson and Schmid, 1983) that consistently shows normal (north side down) displacement, indicating post-thrusting extension of the hanging wall. It cuts into the margin of the outer tonalite ring of the complex in one place on the southern end, resulting in the strain and fabric gradient examined here. Deformation temperatures, as reported below, are approximately 475 ± 50°C. In the following section, we discuss initiation and progressive development of foliation formed in this strain and fabric gradient, focusing on the role played by biotite.

3. Description of the deformation and fabric gradient

Spatially oriented samples were collected at closely-spaced intervals along a transect, starting at the contact between the Cerro de Costilla tonalite and the orthogneiss wall-rocks, and progressing 28.3 m into the tonalite until a point was reached where the rock showed no field evidence of deformation (Fig. 2b). Sample collection was most closely spaced at the edge of the tonalite, where the strongest fabric gradient and mineralogical changes were noted. Two foliation-perpendicular thin sections were prepared from each sample: one parallel to and the other perpendicular to the lineation. Below we describe the progression from the least to most deformed rocks.

Figure 2. Bedding and foliation data in the southern portion of the Cerro de Costilla complex.

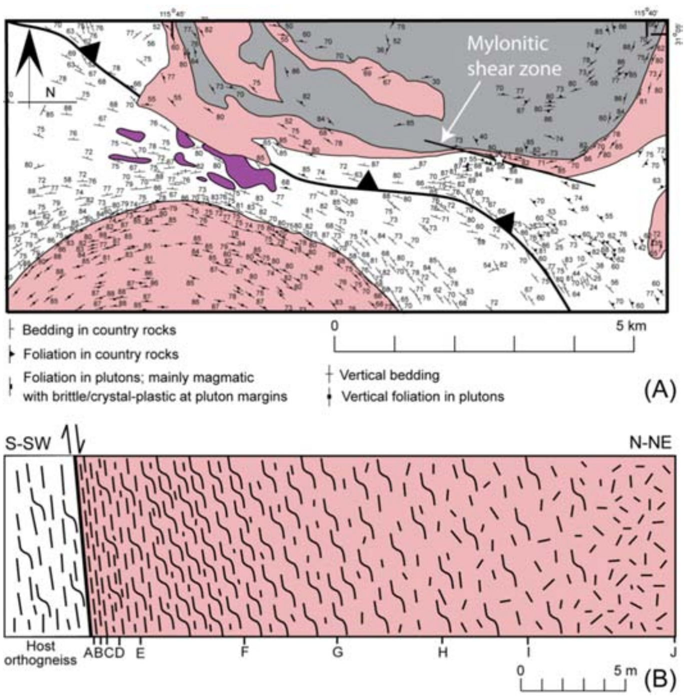

(A) Map showing bedding and foliation data in the southern portion of the Cerro de Costilla complex and surrounding area. See Fig. 1 for geology legend. Data from Johnson *et al.* (2004) and Melis (2006). The mylonitic shear zone examined here is shown at the southern edge of the complex, where it deformed the edge of the outer tonalite ring. Star marks the location where samples were collected. (B) Sketch of 28.3-m transect across the fabric gradient, from the contact with the host orthogneiss to slightly deformed tonalite. Letters A-J correspond to locations of oriented samples referred to in text.

3.1. Least deformed tonalite

The least deformed tonalite observed shows a weak magmatic foliation delineated mainly by biotite aggregates and aligned plagioclase grains. The plagioclase commonly has oscillatory zoning contained within core-to-rim compositional zoning, as discussed in Section 4. It also has well developed growth twinning and a few crystal faces, though most boundaries are irregular. Commonly it contains a few rounded quartz inclusions, as well as local rounded to euhedral and irregularly shaped inclusions of hornblende. Some plagioclase grains have been bent, producing local concentrations of lenticular deformation twins. Local evidence of minor strain-induced grain boundary migration is observed (Fig. 3). Interstitial quartz shows subgrains parallel to the *c*-axis, but has no chess-board subgrain patterns indicative of *c*-slip. It shows evidence of subgrain rotation recrystallization, as well as some grain boundary migration (Fig. 4). Brown-green hornblende occurs as irregularly shaped to subhedral grains and aggregates, some with inclusions of quartz and biotite, together with inclusions of plagioclase that vary from rounded to euhedral with rounded corners. Some of the hornblende has simple or multiple twinning, and some is optically zoned, with brown-green cores and blue-green rims.

Figure 3. Minor grain boundary migration in plagioclase.

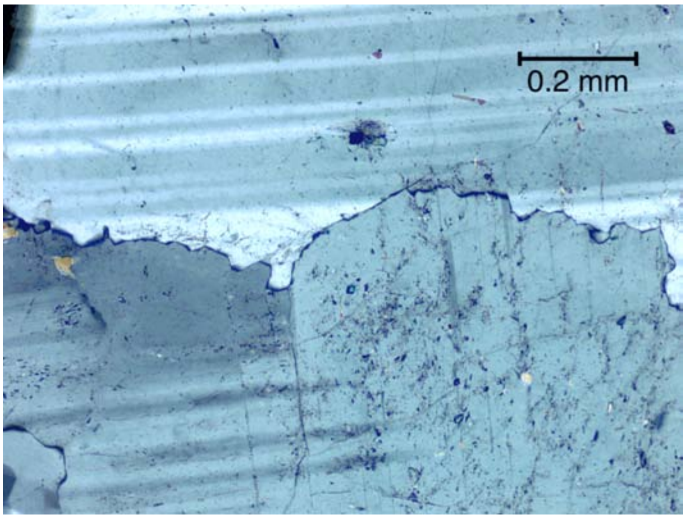

Evidence for minor strain-induced migration of grain boundaries in plagioclase. Crossed polars.

Figure 4. Typical quartz microstructures.

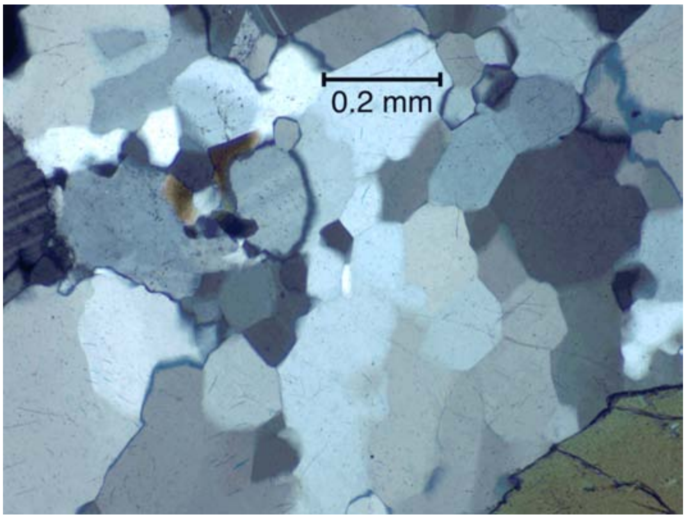

Quartz microstructures typically show evidence for a combination of subgrain rotation recrystallization and minor grain boundary migration. Variably developed foam texture and equilibrium grain boundary geometries indicate post deformational recrystallization. Crossed polars.

Biotite occurs as greenish brown, subhedral grains with {001} faces, as well as 'decussate' aggregates, a few of which locally pass into incipient foliae (Section 4), suggesting that some deformation and recrystallization occurred in the least deformed rocks. Locally biotite is intergrown with hornblende. Some biotite grains are bent, some have slightly misoriented, irregular to ragged 'subgrains' that appear to have been formed by fracturing (Fig. 5), and rare grains have been broken into fragments with ragged edges, the resulting spaces having been filled with quartz, fine-grained titanite and small rotated biotite fragments (Fig. 6). Locally biotite adjacent to plagioclase has been partly replaced by fine-grained, symplectic aggregates of titanite and plagioclase, the plagioclase being commonly in optical continuity with the plagioclase grain on which it nucleated (Fig. 7).

Figure 5. Biotite aggregate in the least deformed tonalite with granular titanite grains.

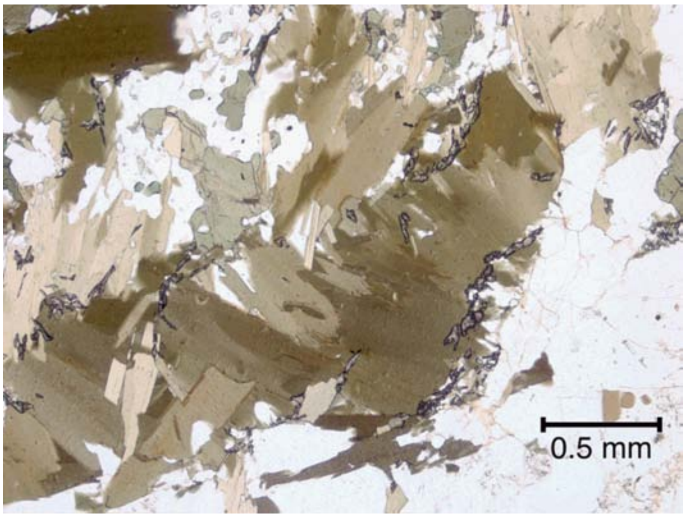

Biotite aggregate in the least deformed tonalite. The splintered grain contains irregular to ragged 'subgrains' with granular titanite concentrated around its edges. Plane-polarized light.

Figure 6. Bent, recrystallized biotite grain.

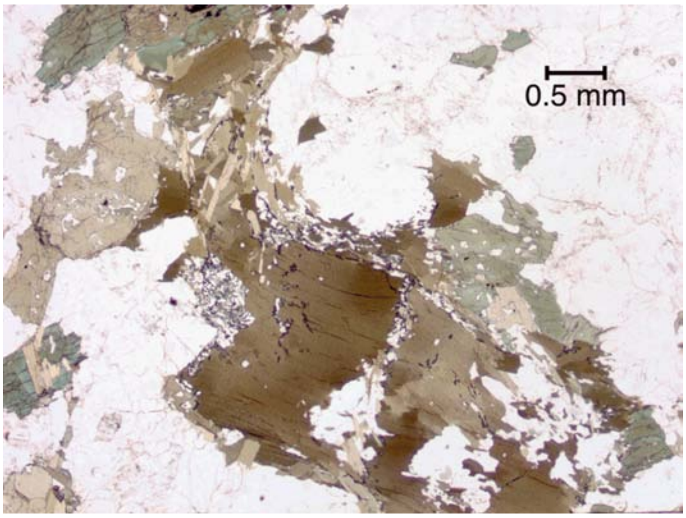

A large biotite grain that has been broken, separated (bottom-center) and bent into a folium and recrystallized (upper-center). The broken edges are ragged, and spaces between adjacent pieces of the original grain have been filled by quartz, fine-grained titanite and small biotite grains. Plane-polarized light.

Figure 7. Biotite partially replaced by symplectic plagioclase and titanite.

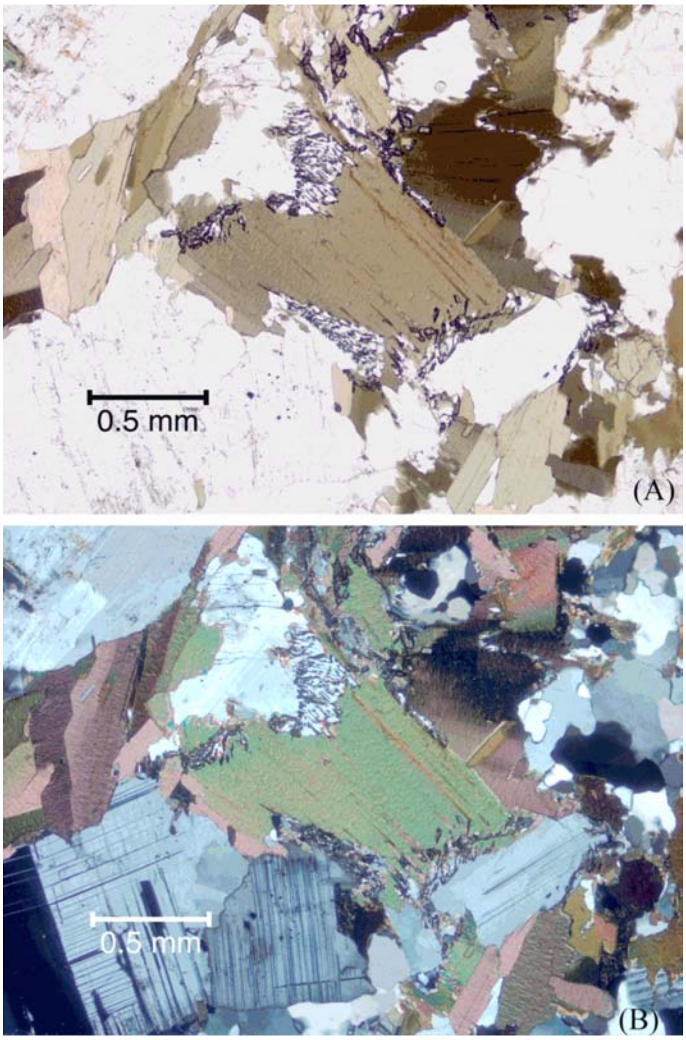

Lobes of symplectic plagioclase and titanite replacing the central biotite. (A) plane-polarized light; (B) crossed polars.

K-feldspar occurs as small interstitial grains marginally replaced by fine-grained myrmekite (Fig. 8), the formation of myrmekite probably being related to the deformation (*e.g.*, Simpson, 1985; Simpson and Wintsch, 1989; Vernon, 1991).

Figure 8. Lobes of fine-grained myrmekite (x) replacing K-feldspar.

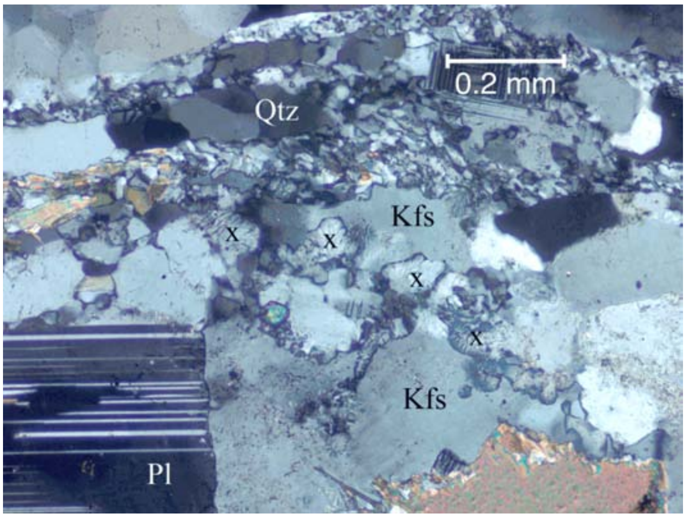

Interstitial K-feldspar (Kfs) extensively replaced by lobes of fine-grained myrmekite (x), which locally has recrystallized to form fine-grained, granular plagioclase-quartz aggregates initiating new foliae (upper half of image). Crossed polars.

Titanite occurs locally as scattered large grains, but mainly as small grains, aligned aggregates and veinlets, especially in biotite. Also present are rare pink to blue-black tourmaline, apatite and brown allanite.

3.2. Initiation of foliae

Quartz recrystallization increases with increasing fabric intensity, though the recrystallized grainsize remains relatively large. The recrystallized aggregates become elongated in more deformed rocks, but are highly elongated only in the most strongly deformed rocks, where they help to delineate the foliation. Quartz also forms incipient foliae in aggregates with biotite (Fig. 9), with or without fine-grained titanite or apatite.

Figure 9. Biotite, plagioclase and quartz forming incipient folium between grains of plagioclase.

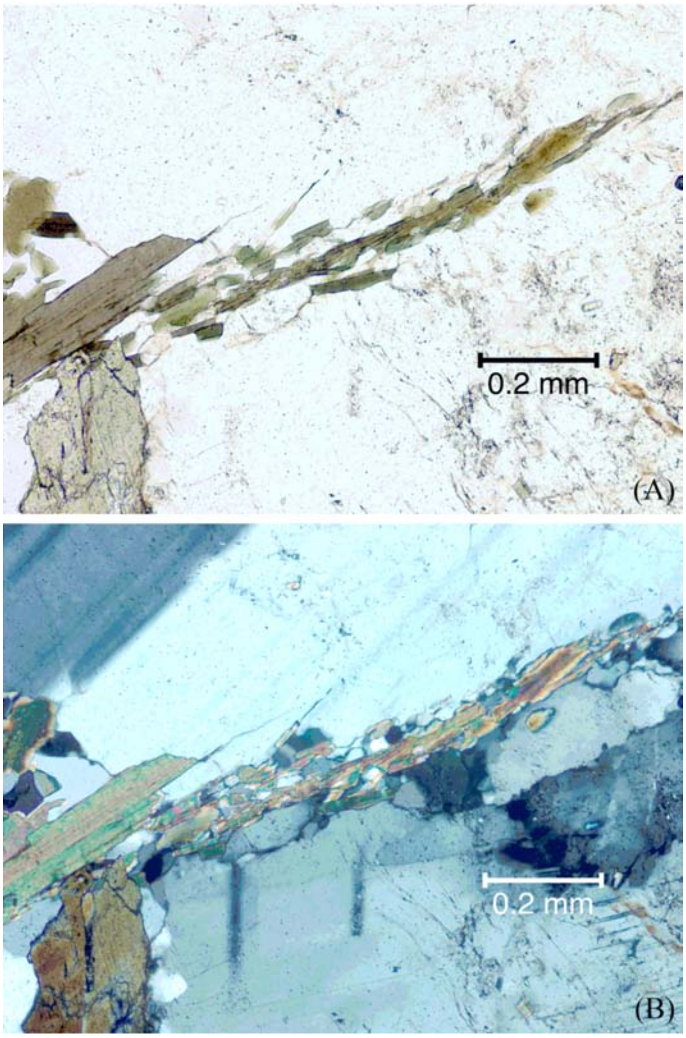

Incipient folium of biotite, plagioclase and quartz between grains of plagioclase that appear to have been either fragmented, recrystallized or both at the lower edge of the folium, which itself appears to have undergone recrystallization to form low-energy grain shapes. Some biotite grains appear to have penetrated along small fractures in plagioclase (centre of image). (A) plane-polarized light; (B) crossed polars.

Plagioclase locally shows small new marginal grains and aggregates of grains that, on the basis of optical evidence, could have been formed by either primary recrystallization or 'sintering' of small fragments. Though apparent subgrains occur locally, deformation temperatures were probably too low for subgrain rotation recrystallization to have played an important role (see sections 3.5 and 4.3). Therefore, local minute subgrains and new grains along internal fractures and grain boundaries (Fig. 10) probably originated mainly as fragments (*e.g.*, Vernon *et al.*, 2004; Johnson *et al.*, 2004), although some genuine subgrains may be present (*e.g.*, Fig. 10a). These fine-grained aggregates may contribute to foliae by providing pathways for linking biotite-rich foliae. Locally plagioclase grains have been fractured and pulled apart, some with fillings of undeformed quartz, others with fillings of recrystallized quartz, others with fillings of quartz and aligned biotite in a crude 'beard' structure, and still others with hornblende and plagioclase fragments that broke away from matrix grains as they flowed in to fill the gap (Fig. 11). No fillings involving feldspar were observed, confirming that melt was absent during the deformation (*cf.* Vernon *et al.*, 2004).

Figure 10. Subgrains and new grains along grain boundaries and fractures in primary plagioclase.

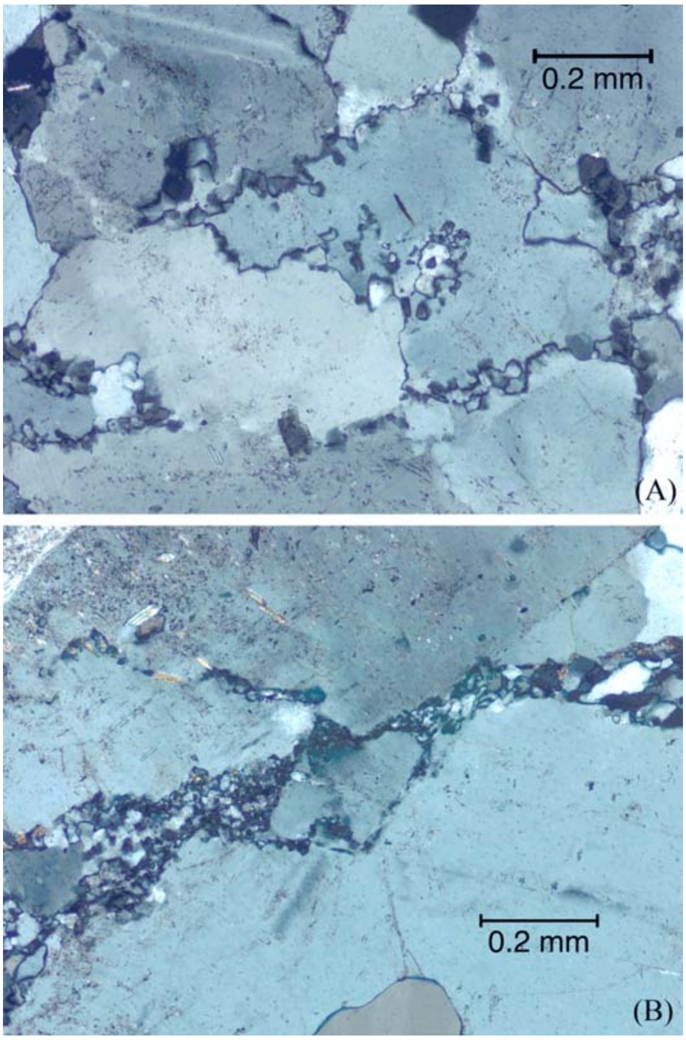

(A) Subgrains and new grains along grain boundaries and fractures in plagioclase. The subgrains and new grains in this example may possibly have formed by subgrain rotation recrystallization, or by fragmentation following by sintering. Crossed polars. (B) Very fine-grained aggregates along fractures in plagioclase, presumably formed by fragmentation. Crossed polars.

Figure 11. A single plagioclase grain broken into three pieces.

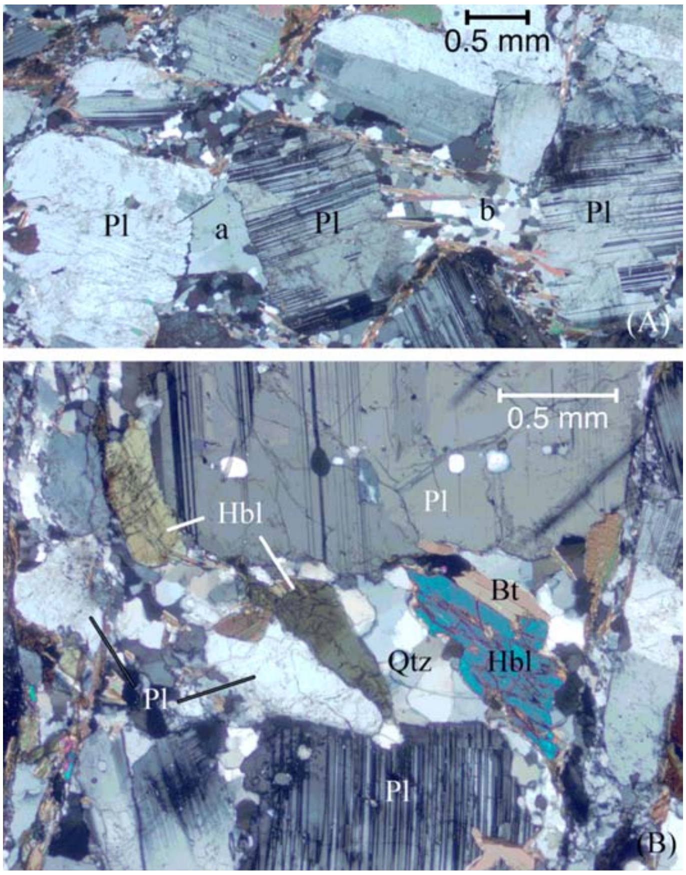

(A) A single plagioclase grain (Pl) broken into three pieces. The left gap contains a pool of only slightly deformed quartz (a) and the right gap contains a 'beard' of recrystallized quartz and aligned biotite. Crossed polars. (B) A plagioclase grain that has been pulled apart, the gap filled with recrystallized quartz, and fragments of hornblende and plagioclase. Lines indicate the matrix grains from which a hornblende (Hbl) and plagioclase (Pl) fragment originated. Crossed polars.

Biotite is the main contributor to foliation initiation, in the form of (1) small biotite grains that grow into fractures on the edges of primary plagioclase grains (Fig. 12a), and are eventually smeared out into long foliae as they separate the plagioclase into pieces (Fig. 12b); (2) aligned biotite aggregates cutting through hornblende grains, some following straight fractures, and others apparently partly replacing hornblende; (3) lenticular biotite grains and aggregates splintering during 'necking down' at their ends to form incipient foliae, owing to sliding of cleavage fragments on one another, followed in some instances by apparent recrystallization (Fig. 13); (4) development of sub-parallel splinters at bends in biotite grains; (5) deformed biotite grains bending into an alignment, accompanied by the development of subgrains and recrystallized aggregates (Fig. 14) (6) biotite-rich foliae leading away from hornblende that was partly replaced by biotite, the foliae commonly carrying small fragments of hornblende (Fig. 15), (7) thin veinlets of very fine-grained biotite and quartz, locally with titanite, epidote or apatite, mostly in primary grain boundaries, though locally cutting through grains, suggesting initiation by fracturing (Fig. 16), (8) 'beards' of biotite and biotite ± quartz on primary plagioclase grains (Figs 11a, 17), and (9) rare biotite splays or fans cut by foliae, to which they contribute (Fig. 18).

Figure 12. Biotite and quartz growing filling fractures in a primary plagioclase grain.

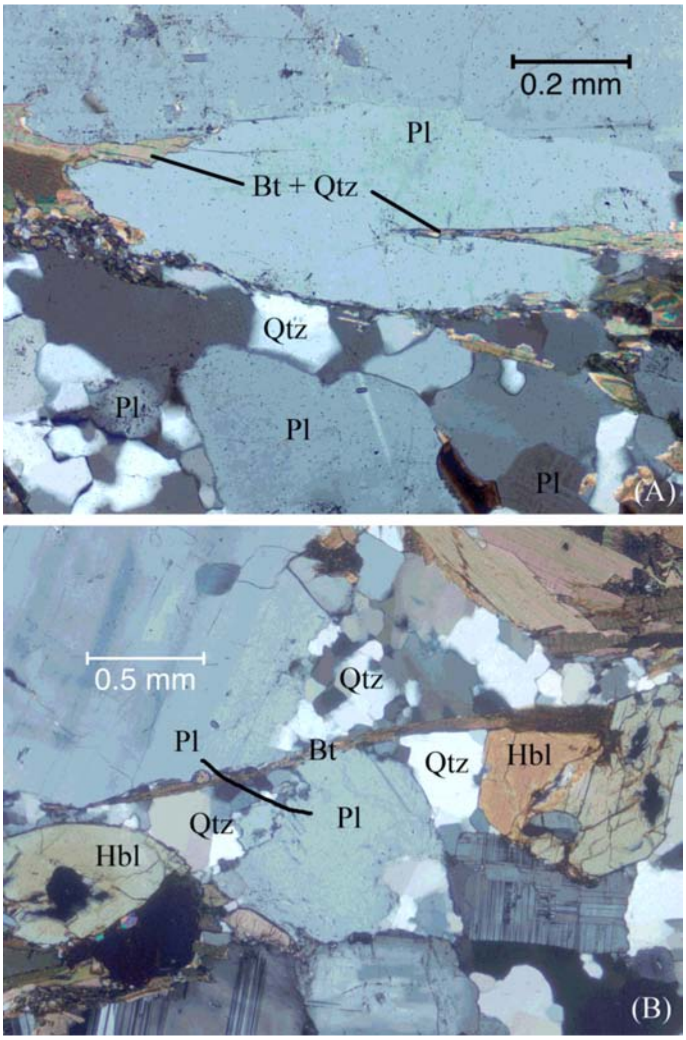

(A) Biotite and quartz growing into fractures on the lower edge of a primary plagioclase grain. Eventually, the lower part of the grain would calve off into the matrix. Fragments of plagioclase (Pl) in the matrix below may also have formed by this process. Crossed polars. (B) An example of what we infer to be a more advanced stage of the process in (A). A plagioclase fragment (lower-center) has been separated from its parent grain. A line shows the plagioclase grains that were once together. Pools of recrystallized quart fill spaces that have developed during the relative motion of strong plagioclase and hornblende (Hbl) grains. Crossed polars.

Figure 13. Thinning and internal deformation of a biotite grain to form a new folium.

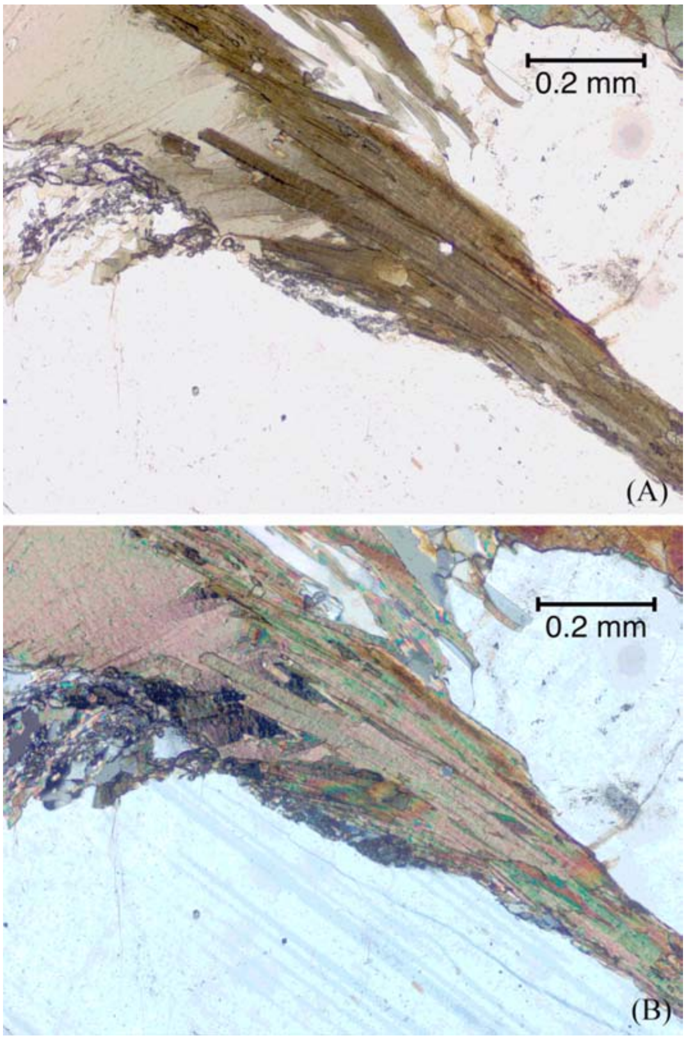

Internally deformed and thinned biotite grain forming an incipient folium between plagioclase grains. (A) Plane-polarized light, (B) Crossed polars.

Figure 14. Biotite grain bent, deformed and recrystallized into a developing foliation.

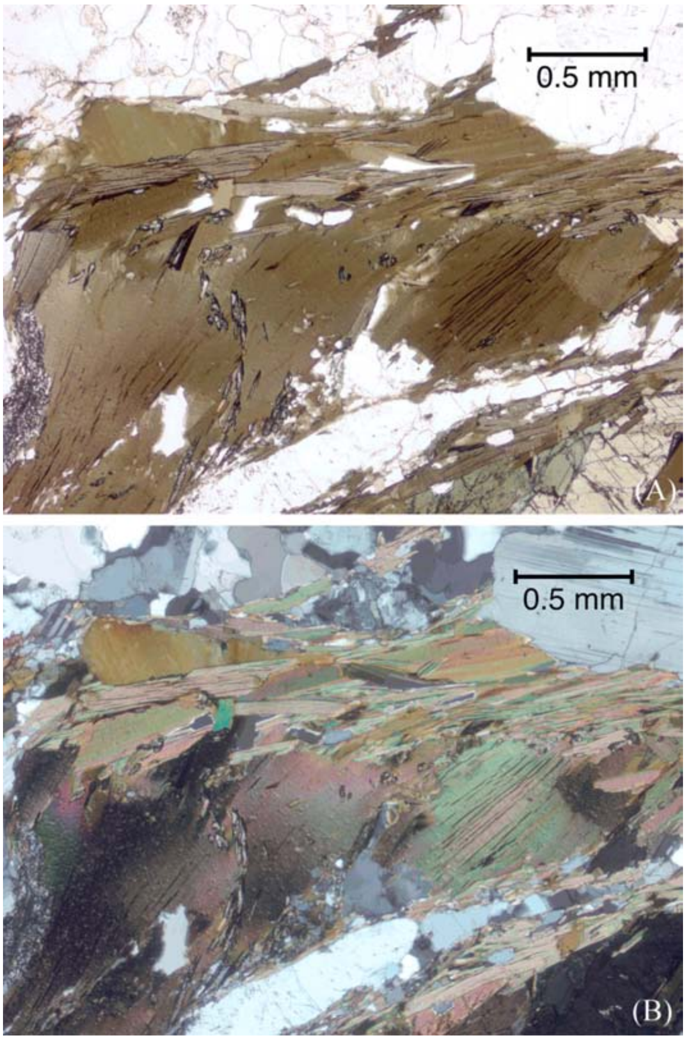

Biotite grain that had been bent towards alignment with a developing foliae, resulting in the development of fractures, subgrains and recrystallized aggregates. (A) Plane-polarized light, (B) Crossed polars.

Figure 15. Hornblende partially replaced by biotite and fragmented into a folium.

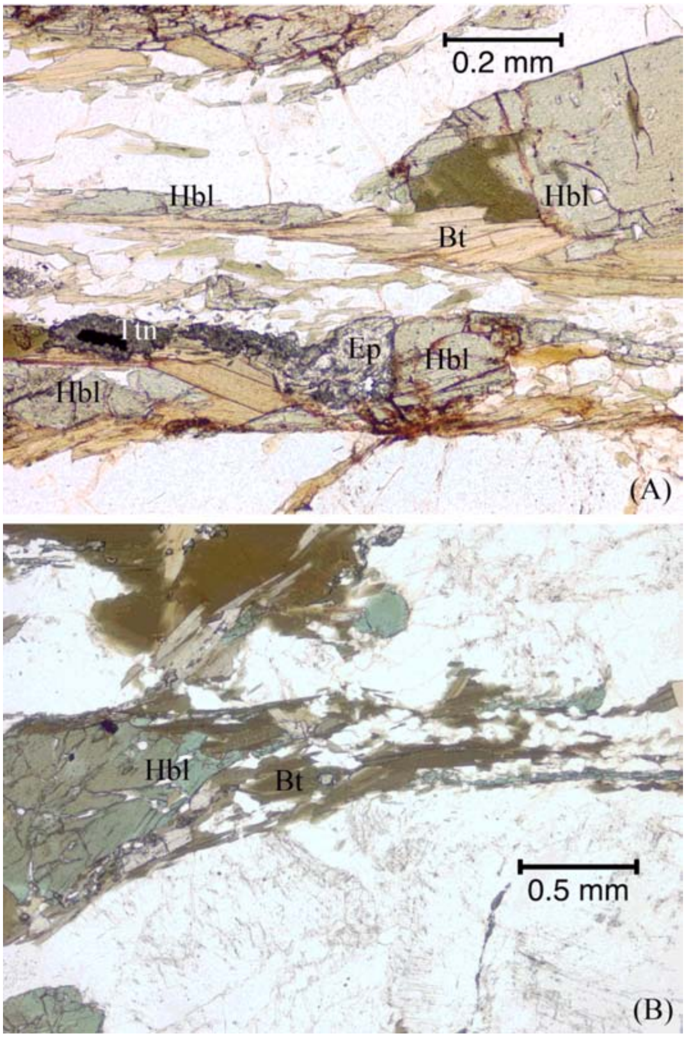

Two examples of extensive replacement of hornblende (Hbl) by biotite (Bt) and developing biotite-quartz folium with small hornblende fragments. (A) and (B) plane-polarized light.

Figure 16. Continuous foliae of biotite and quartz with small fragments of titanite, epidote and hornblende.

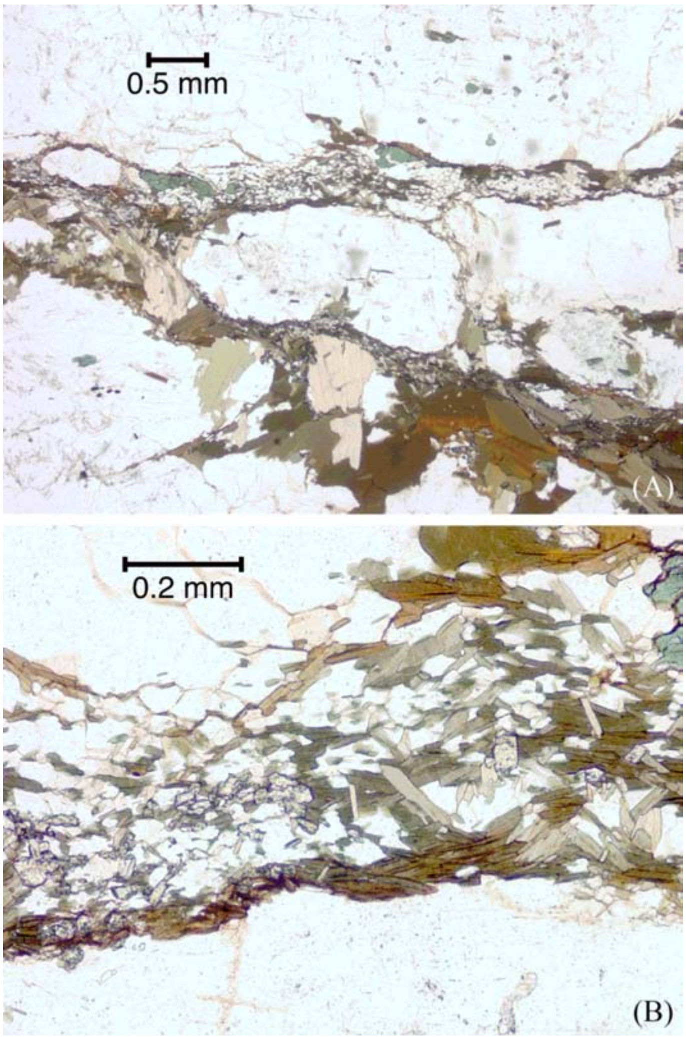

(A) Continuous foliae of biotite and quartz (both mainly recrystallized to form low-energy grain shapes), with small fragments of titanite, epidote and hornblende, anastomosing around large plagioclase grains. Plane-polarized light. (B) Magnified view of part of A, to show quartz and biotite grain shapes. The higher-relief grains are fragments of titanite and epidote. Plane-polarized light.

Figure 17. Biotite and quartz 'beards' on plagioclase

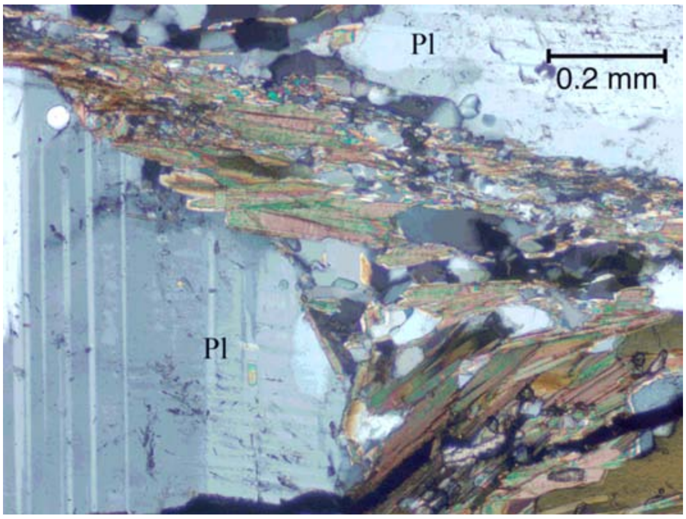

Biotite and quartz 'beards' on plagioclase lead away into foliae, the formation of the 'beards' involving partial replacement of the plagioclase. Crossed polars.

Figure 18. Biotite grain cut through by a foliae to which it contributes by recrystallizing into aligned new grains.

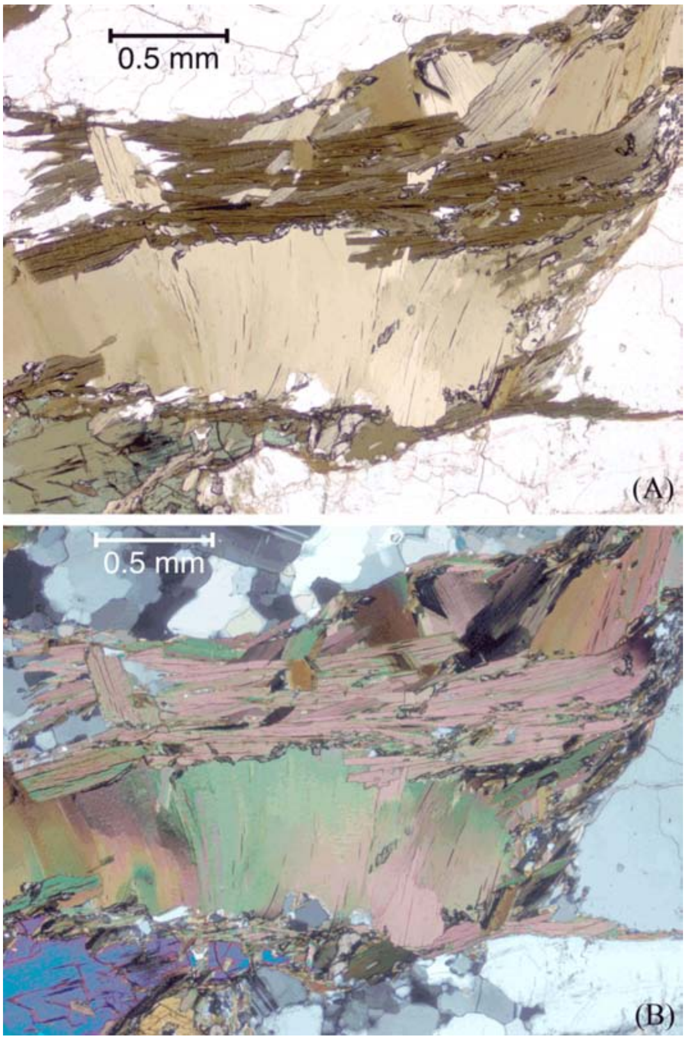

A fan-shaped grain of biotite, cut through by a foliae to which it contributes by recrystallizing into aligned new grains. Grain at lower left is hornblende. (A) plane-polarized light; (B) crossed polars.

Many of the new biotite-rich foliae follow grain boundaries of strong minerals, especially plagioclase and hornblende, constituting the beginnings of an S/C-type foliation pattern (Fig. 19). This is consistent with preferential fracturing along grain boundaries, rather than across grains, though some biotite-rich foliae, apparently occupying former fracture sites, do cut plagioclase and hornblende grains.

Figure 19. Development of an S/C-type fabric around plagioclase grains.

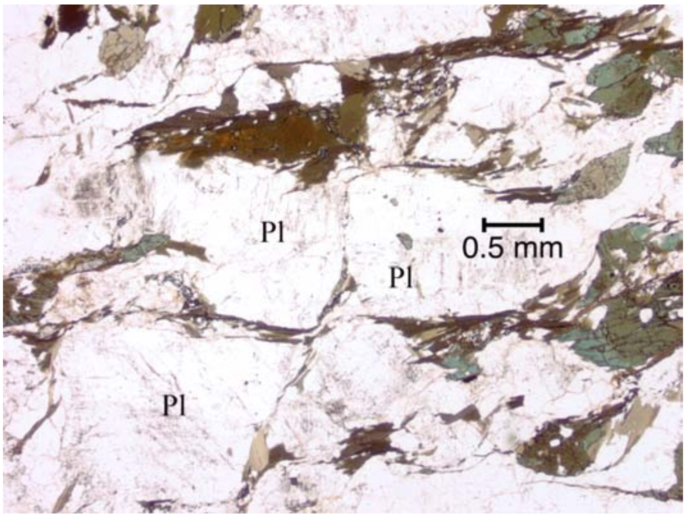

Biotite-rich foliae deflect around plagioclase grains in the beginnings of an S/C-type fabric. Plane-polarized light.

Hornblende shows rare internal deformation in the form of slightly misoriented ‘subgrains’ that probably formed by fracturing. In moderately deformed rocks, ‘beards’ of aligned blue-green hornblende (optically similar to the rims of zoned primary grains), with biotite and quartz, locally develop between drawn apart hornblende fragments (Fig. 20). Where hornblende is extensively replaced by biotite, the resulting hornblende relics can be incorporated into biotite-rich foliae (Fig. 15). Hornblende splinters have locally been smeared, with biotite, along some foliae. Uncommonly, hornblende grains neck down at their ends, releasing small fragments into incipient foliae (Fig. 21). In more strongly deformed rocks, some hornblende grains have been broken into cleavage fragments that have been separated and drawn out into crude foliae, linked by biotite and embedded in recrystallized quartz.

Figure 20. Blue-green hornblende, biotite and quartz form a 'beard' between pulled apart fragments of green-brown hornblende.

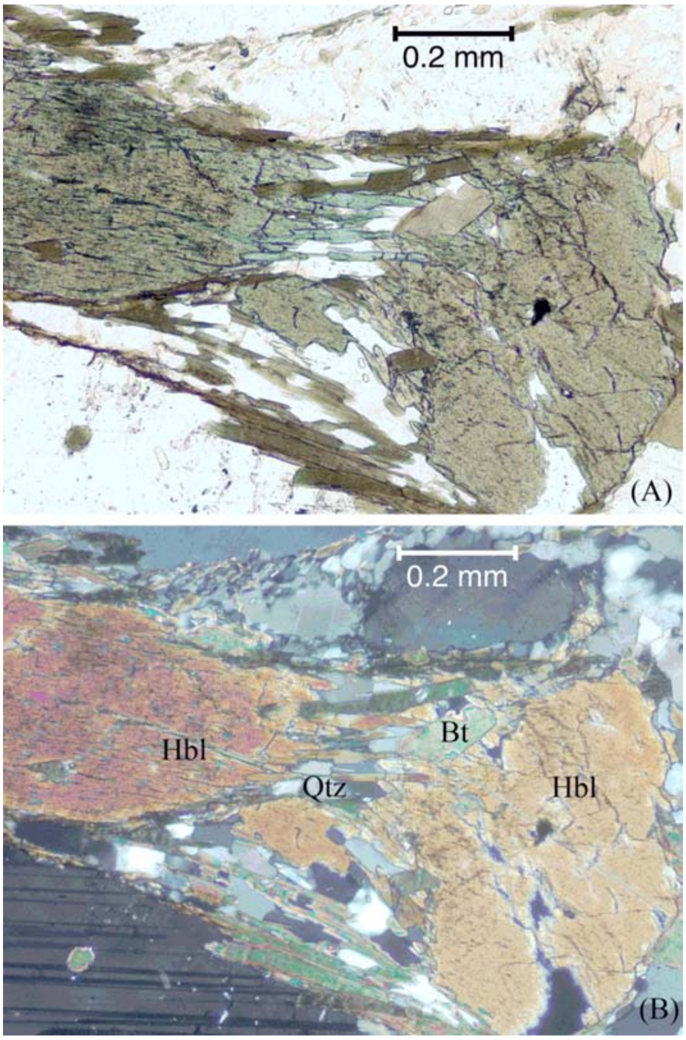

'Beard' of elongate blue-green hornblende, with biotite (Bt) and quartz (Qtz), between pulled apart fragments of green-brown hornblende (Hbl). The relatively low-energy grain shapes of quartz and biotite in the 'beard' suggest some recrystallization. (A) plane-polarized light; (B) crossed polars.

Figure 21. Hornblende grain necked down, fragmented and partly replaced by biotite.

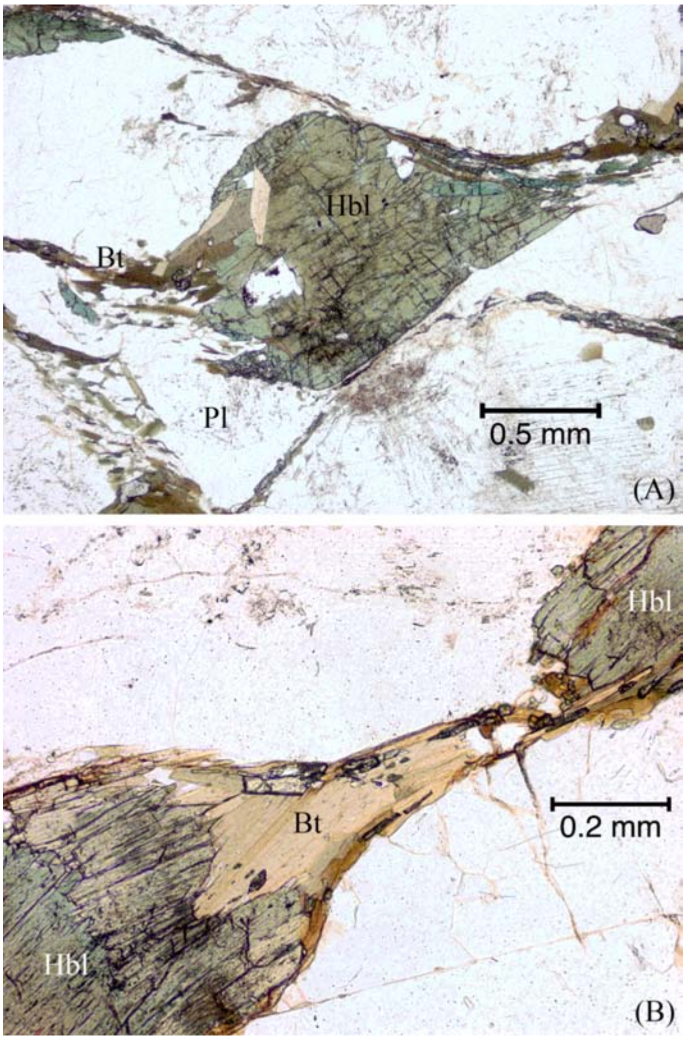

(A) Hornblende (Hbl) grain necking down and partly replaced by biotite (Bt), releasing small splintery hornblende fragments into the developing foliation. Also shown is a biotite-quartz 'beard' on a plagioclase (Pl) grain at bottom-left of image. Plane-polarized light. (B) Hornblende (Hbl) grain that has been boudinaged and pulled apart, and partly replaced by biotite (Bt) that crystallized in the boudin neck. Small fragments of hornblende are incorporated in the biotite. Plane-polarized light.

Titanite makes a minor contribution to the initiation of foliae, in the form of small lozenges and irregular grains in aligned biotite grain boundaries and rare foliae consisting mainly of fragments dislodged from originally large primary titanite grains (Fig. 22). Titanite-plagioclase symplectites replacing biotite (Fig. 7) form a fine-grained reaction product that may help to initiate foliation development, forming recrystallized, fine-grained aggregates (Fig. 23).

Figure 22. Foliae formed mainly of titanite fragments with some quartz and minor biotite.

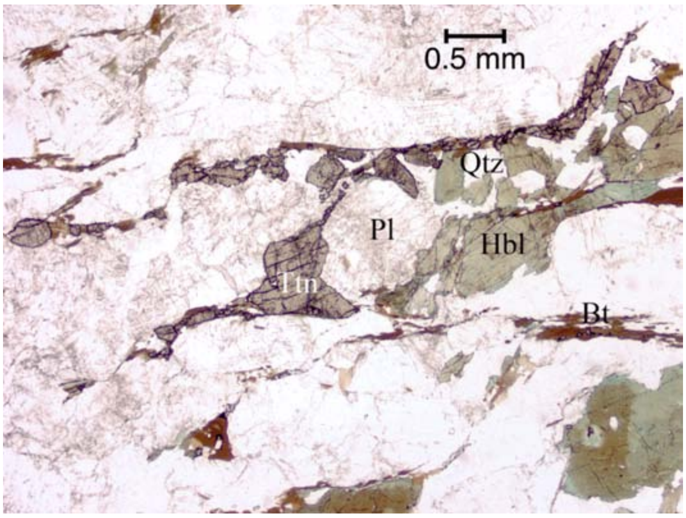

Foliae formed mainly of fragments of titanite (Ttn) with some quartz (Qtz) and minor biotite. Also shown are fragments of hornblende (Hbl) separated by coarse-grained quartz. Plane-polarized light.

Figure 23. Biotite cut by a folium containing titanite and disaggregated plagioclase-titanite symplectite.

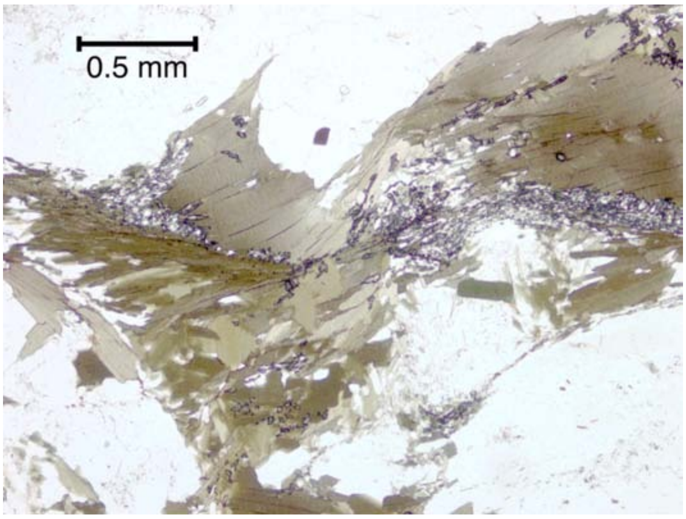

Folium consisting mainly of fine-grained, granular titanite and disaggregated plagioclase-titanite symplectite cutting deformed biotite. Plane-polarized light.

Myrmekite partly replacing the minor amount of interstitial K-feldspar (Fig. 8) can also contribute to the initiation of foliae, because the fine-grained quartz and plagioclase recrystallize to very fine-grained aggregates (Fig. 8) that promote grain-boundary deformation processes (*e.g.*, Vernon *et al.*, 1983; LaTour, 1987).

3.3. More continuous foliae

Many relatively continuous foliae consist of recrystallized biotite ± quartz, with or without irregularly distributed titanite, plagioclase, epidote and hornblende (Fig. 16). In some foliae the biotite is locally ‘decussate’ (Fig. 16), whereas in others it is well aligned (Fig. 15a). Some biotite-rich foliae splay into several foliae. Most foliae pass between primary grains and so tend to anastomose around large, strong grains of plagioclase and hornblende in an S/C-type relationship (Fig. 24).

Figure 24. Anastomosing foliae forming an S/C-type fabric around plagioclase grains.

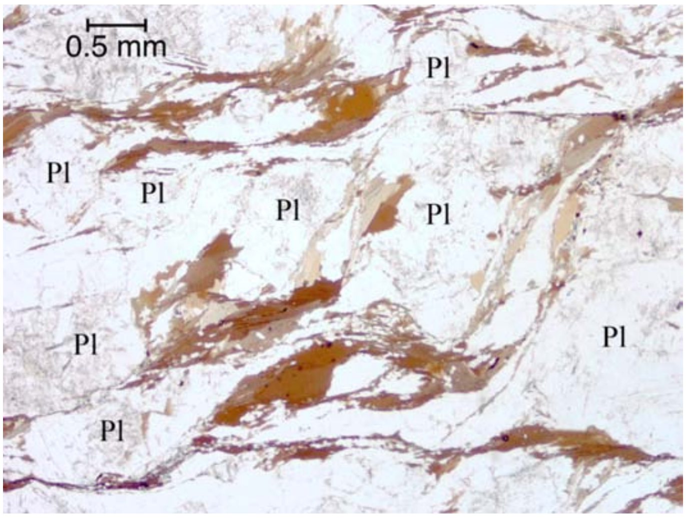

Biotite and biotite-quartz foliae anastomosing around plagioclase grains in an S/C-type relationship (C being parallel to the long edge of the image) in a strongly deformed rock (Sample C). Plane-polarized light.

Initially, the biotite-rich foliae are discontinuous, with insufficient linkages to make a through-going foliation (*e.g.*, Johnson *et al.*, 2004). Links or bridges consist mainly of fine-grained aggregates, with varying proportions of biotite, quartz, titanite and plagioclase (Fig. 25). Some are very fine-grained plagioclase-quartz aggregates representing recrystallized myrmekite (Fig. 8), whereas others appear to be small plagioclase grains, many of which may have originated as minute fragments along fractures (Fig. 10). After the links have been established, further strain can accumulate by preferential deformation of continuous, weak, biotite-rich foliae, producing mylonite, as discussed by Johnson *et al.* (2004).

Figure 25. Fine-grained biotite, plagioclase, quartz and titanite folium linking biotite foliae.

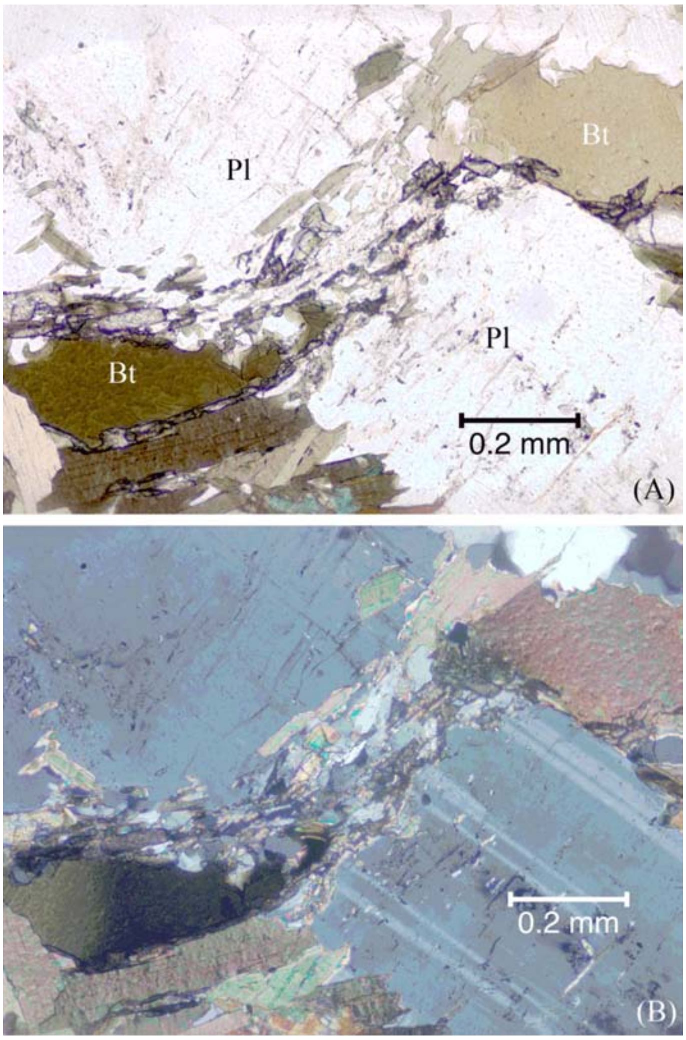

Linking (bridging) folium between biotite foliae, consisting of fine-grained biotite, plagioclase, quartz and titanite. (A) plane-polarized light, (B) crossed polars.

3.4. Strongly deformed rocks

Foliae in the most strongly deformed rocks consist of: (1) continuous aggregates rich in biotite, with varying proportions of quartz, minor ilmenite and rutile, and local fine-grained aggregates derived from the symplectites replacing biotite; (2) elongate aggregates of recrystallized quartz (Fig. 26); and (3) finer-grained aggregates rich in biotite and quartz forming 'beards' on and between plagioclase clasts, all anastomosing around the larger plagioclase grains (Fig. 27). Biotite and, less commonly, quartz appear to have replaced plagioclase at the edges of the 'beards' (Figs 17, 28), although in some instances these minerals may simply be growing into jagged embayments where fragments of the plagioclase have been detached. In many places, these detached plagioclase fragments of various sizes are incorporated into the 'beards' (Fig. 27). We infer that the internal foliation in the 'beards' delineates the stretching direction.

Figure 26. 'Ribbons' of recrystallized quartz

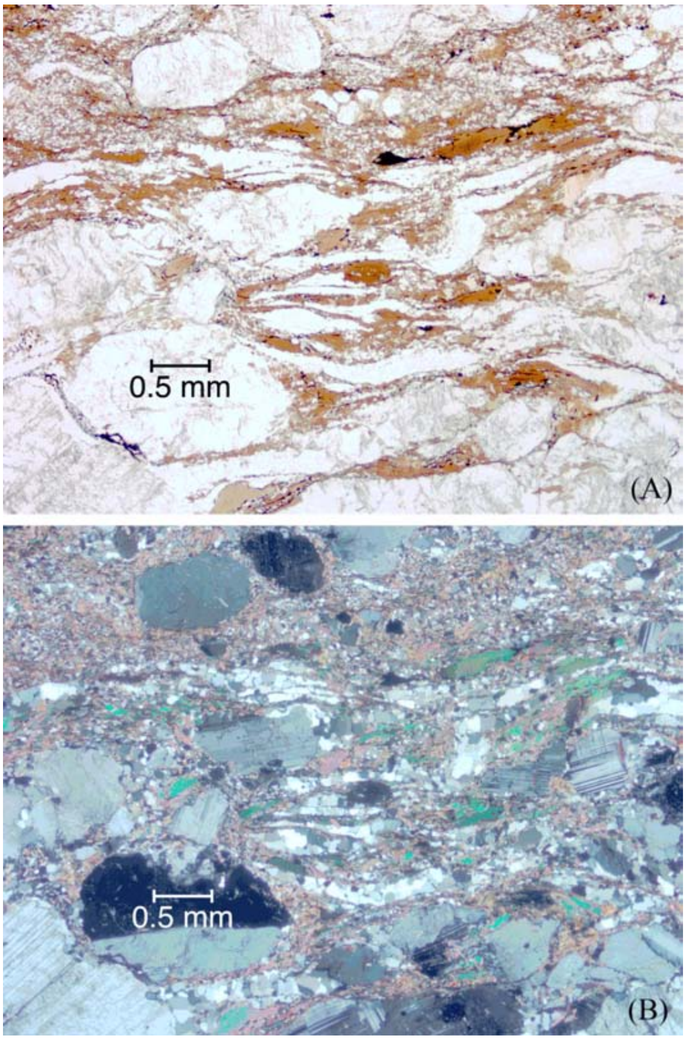

'Ribbons' of recrystallized quartz (representing former interstitial quartz grains) alternating with biotite foliae and biotite-quartz foliae in the most strongly deformed rock (Sample A). (A) plane-polarized light; (B) crossed polars.

Figure 27. Plagioclase clast with 'beard' of biotite and quartz.

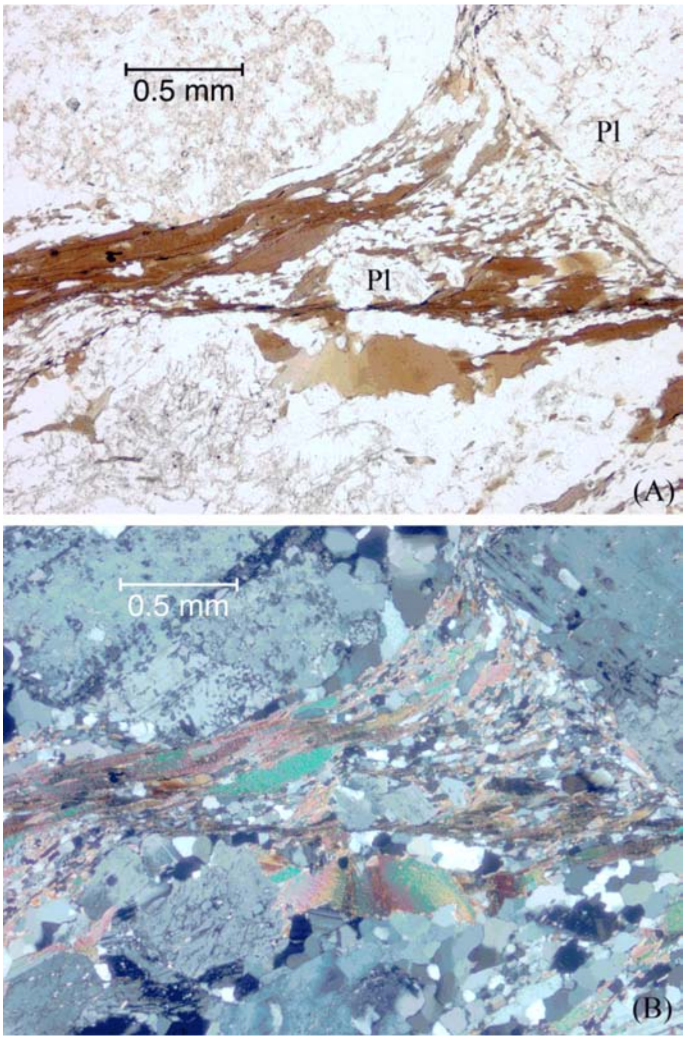

'Beards' of biotite and quartz at the end of a plagioclase clast in a strongly deformed rock (Sample C). (A) plane-polarized light; (B) crossed polars.

Figure 28. Plagioclase clast with 'beard' of biotite and quartz.

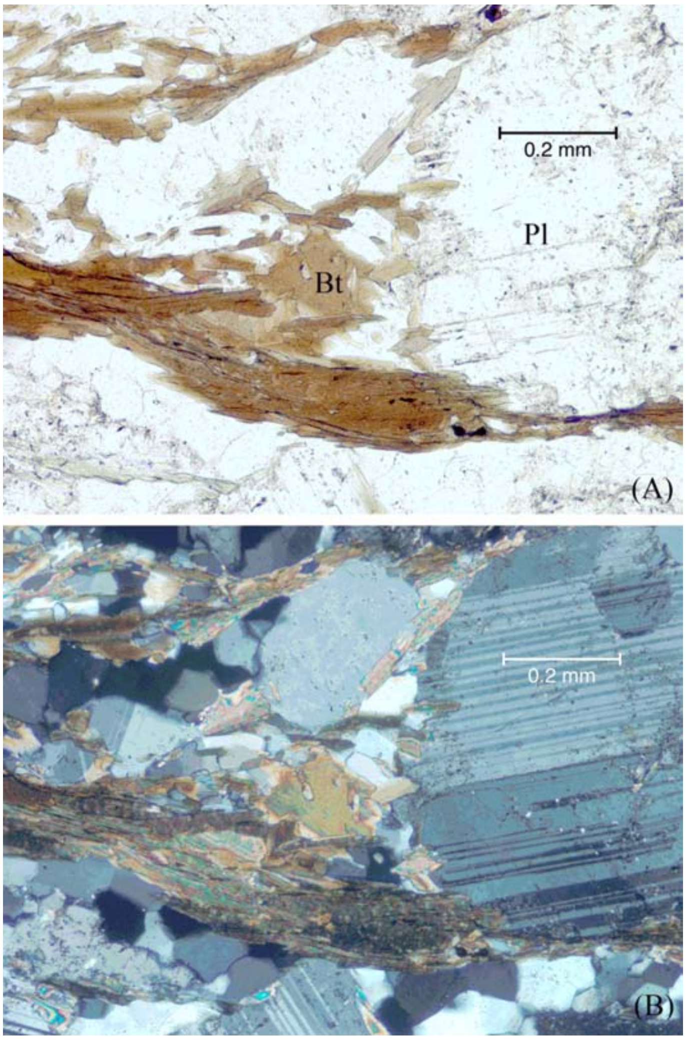

'Beard' of biotite and quartz at the end of a plagioclase clast in a strongly deformed rock (Sample C). The biotite, and possibly quartz, appear to have replaced the plagioclase. (A) plane-polarized light; (B) crossed polars.

As shortening normal to the foliation increases, the plagioclase clasts separate, with the result that the 'beards' become extended into fine-grained, foliated aggregates and continuous fine-grained foliae (Figs 27, 29), eventually constituting a foliated matrix between residual plagioclase clasts. At this stage of foliation development, the S/C-type character of the less deformed rocks is replaced locally by a more uniform, anastomosing foliation as the biotite and quartz foliae collapse into zones between separating plagioclase clasts. The plagioclase clasts are locally broken and can be extensively fragmented, the fragments being cemented by recrystallized quartz (Fig. 30).

Figure 29. Plagioclase clast with 'beard' of biotite and quartz extending into a folium.

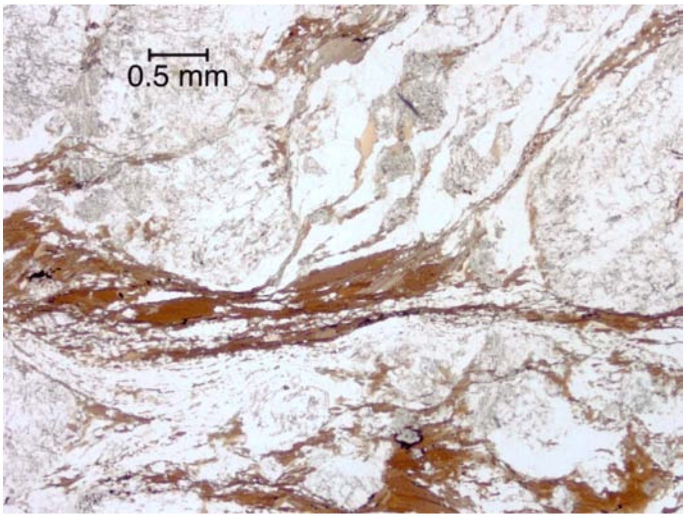

'Beard' extended into a folium in a strongly deformed rock (Sample C). Plane-polarized light.

Figure 30. Shattered plagioclase clast with infilling of quartz.

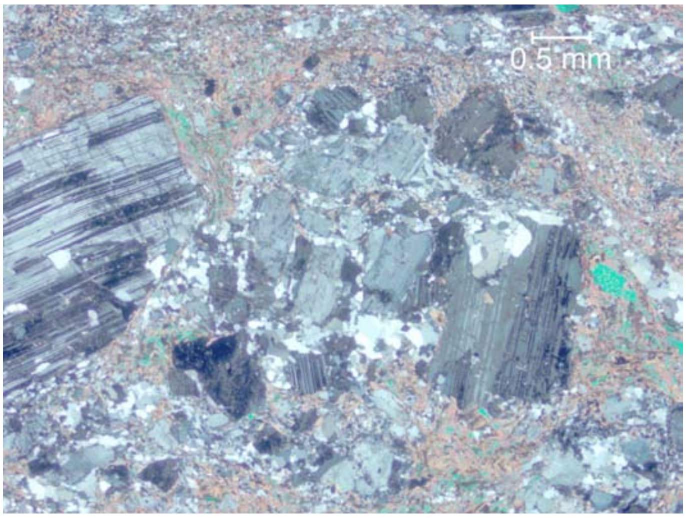

Plagioclase clast that has been shattered, the volumes between the fragments having been filled with quartz, now recrystallized, in the most strongly deformed rock (Sample A). Crossed polars.

In one layer (about 2 cm thick) of one of the more strongly deformed rocks, the plagioclase shows marginal replacement by lobes and irregular patches of symplectic, myrmekite-like aggregates (Fig. 31), some plagioclase grains having been extensively to completely replaced; locally the replacing plagioclase is devoid of quartz blebs (Fig. 31). The rocks show an abrupt change from layers without plagioclase replacement to the layer with extensive plagioclase replacement. We infer that this layer was preferentially infiltrated by fluid, in order to produce the symplectite (discussed below).

Figure 31. Plagioclase-quartz symplectite (x) replacing plagioclase.

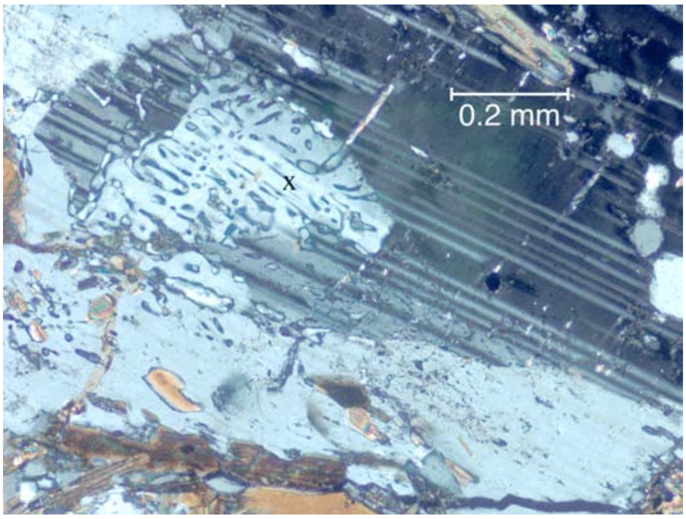

Lobe of plagioclase-quartz symplectite (x) replacing plagioclase in a layer in Sample C. See Fig. 37b for plagioclase compositional data. Crossed polars.

The most deformed rocks (sample A) contain quartz-tourmaline patches and veins, in which the tourmaline occurs as angular fragments dispersed in recrystallized quartz. Some of the tourmaline consists of close fragments that could be fitted back together, separated by single-crystal quartz fillings, suggesting deposition of quartz from solution.

In the mylonitic rock immediately at the edge of the pluton (sample A), the grainsize of the biotite-quartz aggregates is much smaller than in samples B and C, and the amount of matrix between the plagioclase clasts appears to have increased (Fig. 32). Extensive recrystallization of the matrix produced fine-grained decussate aggregates of biotite and aggregates of quartz and biotite with low-energy grain shapes.

Figure 32. Fine-grained, biotite-rich matrix in the most strongly deformed rock.

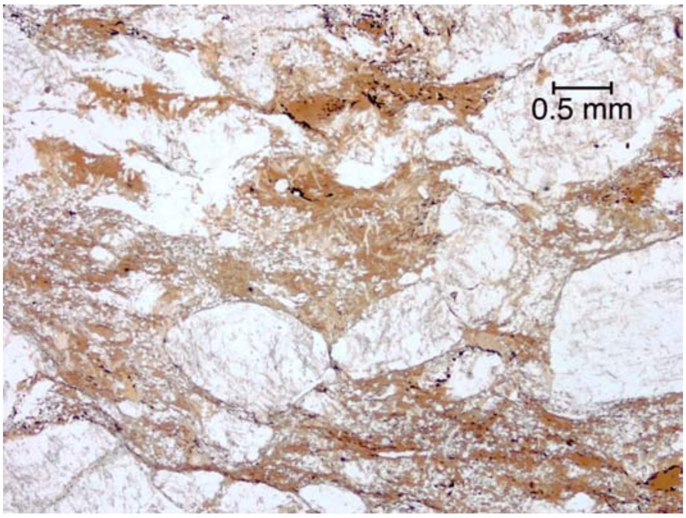

General view of the fine-grained, biotite-rich matrix in the most strongly deformed rock (Sample A). Plane-polarized light.

3.5. Microstructural evidence of deformation conditions

We infer from microstructural observations that the deformation temperatures for the Cerro de Costilla rocks were 400-550°C, because (1) quartz shows no evidence of *c*-slip, which is generally inferred to require temperatures above 600°C (*e.g.*, Kruhl, 1996, 1998); (2) quartz shows widespread evidence of subgrain rotation recrystallization, and some evidence for grain-boundary migration recrystallization, suggesting a temperature range of 400-500°C (Hirth and Tullis, 1992; Tullis *et al.*, 2000; Stipp *et al.*, 2002a, b); and (3) plagioclase shows no clear evidence of dislocation creep or subgrain rotation recrystallization, which require temperatures above 500-550°C (Tullis *et al.*, 2000; Rosenberg and Stünitz, 2003); instead it appears to have undergone minor grain-boundary migration and fracturing, though some recrystallization ('sintering') of fragmental aggregates may have occurred — a process that can occur at less than 400-500°C (Fitz Gerald and Stünitz, 1993). Given the local mobility of plagioclase grain boundaries, and that we cannot completely rule out very rare subgrain development through rotation recrystallization, we place an upper limit on temperature of 550°C. In Section 4.3 we present hornblende-plagioclase thermometry that suggests a deformation temperature less than approximately 540°C. In view of the microstructural evidence and thermometry results, we suggest that the deformation temperature was 475 ± 50°C.

4. Geochemistry

In this section we present whole-rock and mineral chemical data from samples collected across the pluton margin. Additionally, we estimate the degree to which metasomatic alteration and volumetric strain accompanied deformation, and present the generalized metamorphic reactions inferred from the observed mineralogical and microstructural changes.

4.1. Whole-rock chemistry

The bulk chemical composition of samples from the marginal Cerro de Costilla tonalite was analysed by ICP-MS at Activation Laboratories, Ontario, Canada to evaluate possible chemical variability associated with the deformation gradient (Table 1). Samples were collected at progressively smaller intervals from the undeformed interior (samples H-J), through progressively more deformed rocks (samples D-F), into the highly-sheared margin (samples A-C).

Figure . **Table** 1.

Rock Type	Host orthogneiss	Cerro de Costilla Sheared margin			Cerro de Costilla Interior					Domain Totals				% Gains/Losses from interior
Sample	PVS (avg)	A*	B	C	D	E	F	H	J	B-C		D-J		
wt%										Avg	S.D.	Avg	S.D.	
SiO_2	71.84	65.35	66.99	67.48	63.48	63.55	62.77	62.86	62.19	67.24	0.35	62.97	0.56	15.2
Al_2O_3	14.77	17.03	15.76	15.52	16.59	16.12	16.37	16.38	16.58	15.64	0.17	16.41	0.19	-
$Fe_2O_{3(T)}$	2.66	4.64	3.96	4.01	5.00	4.84	5.08	5.00	5.26	3.99	0.04	5.04	0.15	-14.4
MnO	0.06	0.06	0.06	0.07	0.08	0.08	0.08	0.02	0.08	0.07	0.01	0.07	0.03	5.5
MgO	0.56	2.64	2.38	2.42	3.05	2.91	3.09	3.24	3.16	2.40	0.03	3.09	0.12	-16.6
CaO	2.58	4.28	4.05	4.02	5.34	5.25	5.40	5.41	5.43	4.04	0.02	5.37	0.07	-20.4
Na_2O	3.54	3.16	2.87	2.81	3.78	4.01	3.95	3.92	3.87	2.84	0.04	3.91	0.09	-24.6
K_2O	3.11	2.11	1.96	2.07	1.60	1.58	1.64	1.70	1.78	2.02	0.08	1.66	0.08	25.4
TiO_2	0.27	0.57	0.49	0.55	0.67	0.63	0.69	0.70	0.74	0.52	0.04	0.69	0.04	-
P_2O_5	0.08	0.20	0.14	0.12	0.14	0.15	0.15	0.17	0.16	0.13	0.01	0.15	0.01	-7.3
LOI	NA	0.95	0.78	0.82	0.75	0.64	0.77		0.75	0.80	0.03	0.73	0.06	17.6
Total	99.47	101.00	99.43	99.89	100.50	99.77	99.99	99.39	99.99	99.67	0.33	100.07	0.40	-
ppm														
Ba	956	456	483	511	458	428	460	563	493	497	19.8	480	51.6	12.5
Sr	202	315	298	309	418	417	417	400	417	304	7.8	414	7.7	-23.5
Y	21	6	18	19	16	13	18	16	12	19	0.7	15	2.4	26.6
Sc	NA	12	11	10	13	12	14	15	12	11	0.7	13	1.3	-13.8
Zr	126	41	117	132	135	132	179	117	148	125	10.6	142	23.3	-
Be	NA	1	2	2	1	1	1	2	2	2	0.0	1	0.5	36.6
V	25	102	80	87	108	101	108	116	117	84	4.9	110	6.6	-19.3
ρ	NA	-	2.75	2.71	2.78	-	-	2.75	-	2.73	0.03	2.76	0.02	-

Whole-rock geochemistry and calculated bulk compositional changes in the sheared margin of the tonalite (samples B & C) based on Isocon method. PVS = published data for Pine Valley Suite orthogneisses (Todd *et al.*, 2003). Densities calculated from sample mode and measured mineral compositions.

Samples from the less deformed rocks (D-J) have a relatively uniform, tonalitic bulk composition. Within ~1 m of the contact with the wall-rock granitic orthogneiss, a sharp change occurs in most major and trace element concentrations (Fig. 33). Samples B and C have much lower concentrations of Na_2O, MgO, CaO, Fe_2O_3, and Al_2O_3, and higher SiO_2, K_2O, and LOI (taken as H_2O) than samples D – J (Fig. 33). Sample A, collected within 10 cm of the host rock contact, has markedly more Na_2O, MgO, CaO, Fe_2O_3, and Al_2O_3, and less SiO_2, Y, Zr, and V, relative to adjacent samples B and C. The presence of cm-scale quartz and tourmaline-rich veins near the host rock contact suggests that this 10-20 cm wide zone may have been subject to additional fluxing of fluids, possibly with different compositions, compared with the more interior marginal samples (B and C). Sample A is therefore excluded from mass balance calculations presented below.

Figure 33. Bulk chemistry from interior to margin of the shear zone.

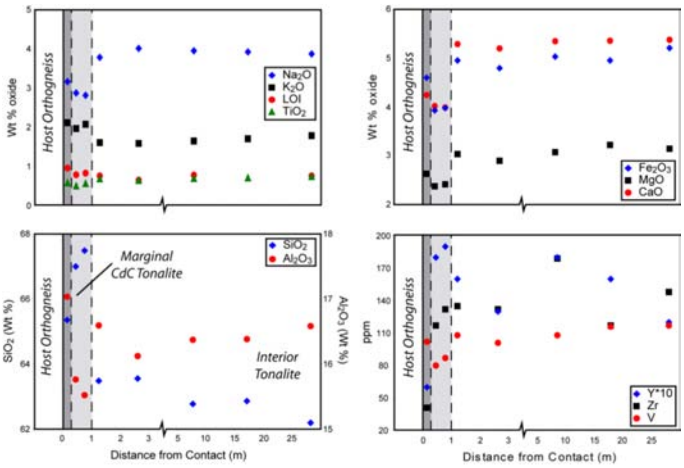

Spatial variation in bulk chemistry from interior to margin of the shear zone. Note the substantial changes in chemistry within c. 1 m of the contact with the host orthogneiss.

4.1.1. Mass-balance and volumetric strain

The relative changes in whole-rock major and trace element concentrations between the unaltered protolith (samples D-J) and the sheared marginal rocks (B and C) are evaluated using the Isocon method (Grant, 1986, 2005). The choice of a reference isocon is often problematic, and can be based on some combination of petrographic observations, statistical methods, and experimental determination of elemental behavior (see Baumgartner and Olsen, 1995 and Grant, 2005 for reviews). Low solubility and/or high field strength elements (*e.g.*, Al, Ti, and Zr) are commonly assumed to be relatively immobile in metasomatic environments (*e.g.*, Ague, 1994, Lonka *et al.*, 1998, Barnes *et al.*, 2004; Grant, 2005), although several examples of mobility of these elements have been described (*e.g.*, Lafrance & Vernon, 1993, 1999; McLelland *et al.*, 2000a, 2000b; Barnes *et al.*, 2004). For this study, we select a best-fit isocon through Al_2O_3, TiO_2, and Zr that has an excellent correlation (R^2 = 0.988) and is consistent with suspected major element gains (SiO_2, K_2O, and H_2O) and losses (Na_2O, MgO, CaO, Fe_2O_3) based on petrographic observations and chemical data (Fig. 34). The relative enrichment and depletion of major elements calculated from the immobile element isocon are presented in Table 1, and show a ~15%-25% change in each of the mobile major oxides.

Figure 34. Isocon plot of average interior and marginal bulk compositions across the shear zone.

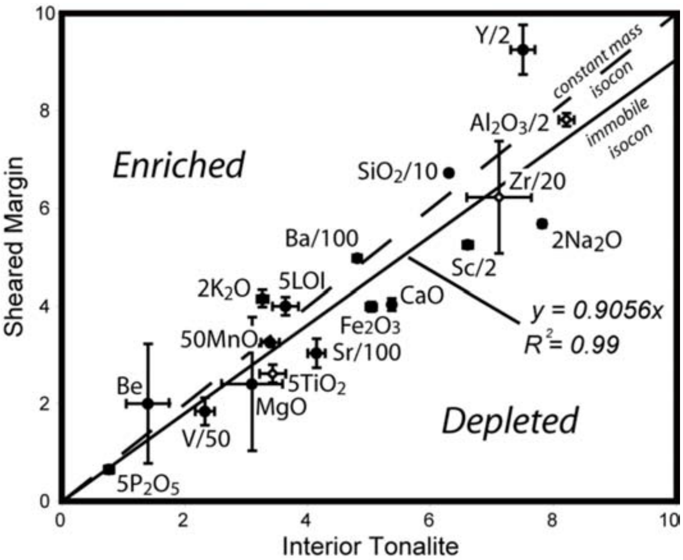

Isocon plot of average interior and marginal bulk compositions across the shear zone. Note the enrichment in K_2O, SiO_2, and LOI, and depletion in Fe_2O_3, CaO, and Na_2O within the sheared margin relative to the immobile isocon.

The slope of the isocon (0.9056) indicates an overall mass gain of ~10% during metasomatic alteration of the tonalitic protolith (Grant, 1986). The equation:

$$\frac{V_a}{V_o} = \left(\frac{M_a}{M_o}\right) \times \left(\frac{\rho_o}{\rho_a}\right)$$

(Grant, 1986) yields an approximate volumetric strain of +12 %, owing to the minor decrease in the average densities (Table 1) of altered samples (B and C), relative to protolith samples (D and H), as calculated from modes (Table 2). Thus, a dilational component of deformation in the pluton margin is inferred from the mass-balance evidence.

Figure . Table 2.

Sample	B	C	D	H
modal%				
Qtz	33.9	37.8	22.5	22.3
Plag	43.8	46.2	50.4	55.1
Amp	0.0	0.0	12.2	11.1
Bt	20.8	15.4	14.2	10.4
Kfs	0.2	0.1	0.0	0.5
Ttn	0.2	0.1	0.4	0.4
FeOx	0.9	0.3	0.2	0.0
Total	100	100	100	100

Modal mineralogy of samples collected across the shear zone.

4.2. Mineral chemistry and inferred reactions

In addition to the microstructural and bulk chemical changes across the sheared pluton margin, systematic changes in plagioclase, biotite, and hornblende composition are also observed (Fig. 35, Table 3). The major modal changes from the undeformed interior to the most deformed rocks are shown in Fig. 36 and include: a steady decrease in plagioclase, a sharp decrease in hornblende, and substantial increases in biotite and quartz in marginal samples (Table 2). Equations intended to represent localized mass transfer or reactions inferred from petrographic observations and associated compositional changes in plagioclase, biotite, and hornblende are discussed below.

Figure . Table 3.

Sample	H				D					C			B		
Phase	Pl		Amp	Bt	Pl		Amp		Bt	Pl		Bt	Pl		Bt
	coarse	matrix			coarse	matrix	coarse	matrix		coarse	matrix		coarse	matrix	
wt%															
Na_2O	7.13	8.09	1.23	0.06	6.83	7.41	0.80	0.59	0.08	6.72	6.91	0.08	6.11	6.01	0.17
K_2O	0.22	0.16	0.82	9.81	0.40	0.11	0.60	0.31	9.47	0.16	0.11	9.68	0.09	0.08	9.25
MgO	0.00	0.01	11.79	11.97	0.00	0.00	12.21	12.97	11.58	0.00	0.00	11.53	0.00	-0.01	11.76
CaO	7.50	6.09	11.60	0.01	7.80	7.19	11.79	11.83	0.01	8.43	8.13	0.00	9.33	9.58	0.14
MnO	0.00	0.00	0.40	0.25	0.01	0.00	0.44	0.42	0.22	0.00	0.00	0.28	-0.01	0.01	0.21
FeO	0.10	0.11	16.02	18.24	0.05	0.11	15.10	14.31	18.35	0.02	0.06	17.09	0.04	0.15	16.75
Al_2O_3	25.55	24.38	8.41	15.72	25.59	25.15	7.70	6.87	16.61	26.33	26.15	17.40	26.89	27.19	17.85
SiO_2	59.67	61.99	45.36	37.59	59.39	60.22	47.16	50.43	37.44	58.73	59.38	36.88	57.38	57.09	37.59
TiO_2	-	-	1.49	2.16	-	-	1.10	0.23	2.11	-	-	2.41	-	-	2.10
Total	100.19	100.86	99.34	100.32	100.12	100.22	99.11	100.11	100.50	100.41	100.76	100.00	99.90	100.12	100.52
apfu															
Na	0.62	0.68	0.36	0.02	0.59	0.63	0.23	0.17	0.02	0.58	0.59	0.02	0.53	0.52	0.02
K	0.01	0.01	0.16	1.89	0.02	0.01	0.11	0.06	1.82	0.01	0.01	1.86	0.01	0.00	1.79
Mg	0.00	0.00	2.64	2.69	0.00	0.00	2.71	2.81	2.60	0.00	0.00	2.59	0.00	0.00	2.66
Ca	0.36	0.29	1.87	0.00	0.37	0.34	1.88	1.84	0.00	0.40	0.39	0.00	0.45	0.46	0.00
Mn	0.00	0.00	0.05	0.03	0.00	0.00	0.06	0.05	0.03	0.00	0.00	0.04	0.00	0.00	0.03
Fe	0.00	0.00	2.01	2.30	0.00	0.00	1.88	1.74	2.31	0.00	0.00	2.15	0.00	0.01	2.13
Al	1.34	1.27	1.49	2.80	1.35	1.31	1.35	1.18	2.94	1.38	1.37	3.09	1.42	1.44	3.11
Si	2.66	2.72	6.81	5.67	2.65	2.69	7.02	7.32	5.63	2.61	2.63	5.56	2.57	2.56	5.57
Ti	-	-	0.17	0.25	-	-	0.12	0.03	0.24	-	-	0.27	-	-	0.24
Total	4.99	4.99	17.56	19.68	4.98	4.98	17.37	17.19	19.63	4.99	4.99	19.62	4.98	4.99	19.60
X Ca	0.37	0.30			0.39	0.35				0.41	0.39		0.46	0.47	
X Mg			0.57	0.54			0.59	0.62	0.53			0.55			0.56
Al (VI)			0.30	0.47			0.37	0.50	0.57			0.64			0.68
n	6	7	6	7	4	5	4	5	9	4	2	9	3	4	9

Mineral chemistry of major phases in the Cerro de Costilla tonalite.

Figure 35. Chemistry of major minerals across the shear zone.

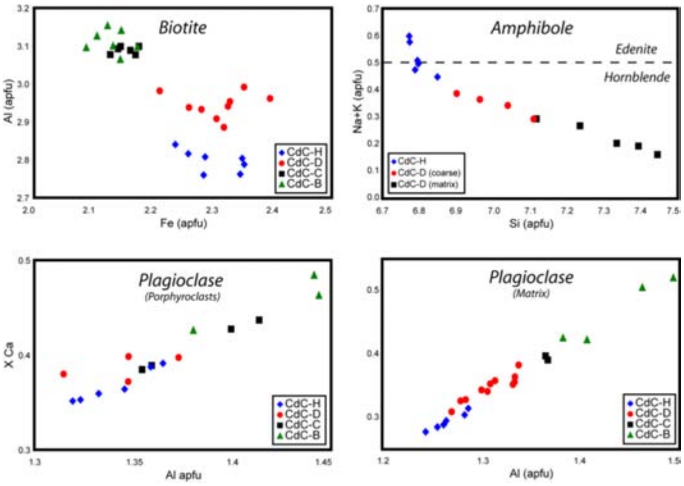

Chemistry of major minerals in samples B, C, D and H.

Figure 36. Modal mineralogy from the interior to the margin of the shear zone.

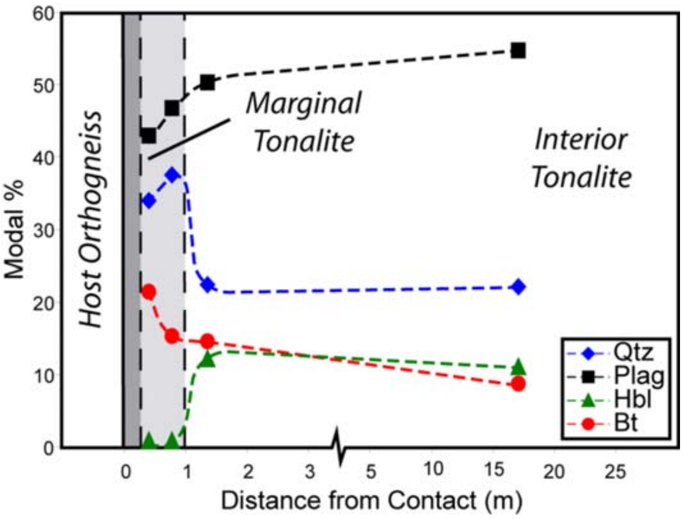

Spatial variation in modal mineralogy from the interior to the margin of the shear zone. Note the marked changes in modal mineralogy within ~ 1m of the contact with the host orthogneiss.

4.2.1. Plagioclase

In the least deformed tonalite, coarse-grained plagioclase preserves its original magmatic compositional zoning, with X_{Ca} fluctuating by up to 0.10 within single grains, and an average of 0.37. Small plagioclase grains are typically unzoned and consistently more sodic than the larger zoned grains, with an average X_{Ca} of 0.30 (Fig. 35).

Close to the pluton margin, coarse-grained plagioclase is generally more calcic; however, a large degree of compositional overlap exists between samples. Compositional changes in the matrix (recystallized) plagioclase are more systematic, with a clear positive correlation between Ca content and proximity to the pluton margin (Fig. 35). The matrix plagioclase in sample B (~40 cm from the contact) has an average X_{Ca} of 0.47, up substantially from that of interior sample H (~X_{Ca} = 0.30). Higher Ca concentrations in the matrix plagioclase probably reflect the breakdown of calcic amphibole, the generally more calcic composition of the primary plagioclase grains that recrystallized/neocrystallized to form the matrix grains, and the possibility of preferential leaching of Na in comparison to Ca during metasomatic alteration (discussed below).

Symplectic intergrowths of fine-grained plagioclase, titanite and new biotite, and of myrmekite-like plagioclase and quartz, are observed locally replacing coarse grained (primary) biotite and plagioclase, respectively. The symplectic structure reflects simultaneous growth of all three minerals, and we infer that the reaction occurred in response to, or was assisted by, the deformation and enhanced element mobility. The composition of symplectic plagioclase intergrown with titanite is similar to that of the coarse grained (porphyroclastic) and matrix plagioclase (*i.e.*, in the range of X_{Ca} = 0.30-0.40), but is locally of slightly different composition from its host grain (Fig. 37a). We infer that these symplectic intergrowths of fine-grained plagioclase, titanite and new biotite are produced by a reaction represented by the generalized equation:

$$Bt_1 + Pl_1 = Ttn + Pl_2 + Bt_2$$

and their widespread occurrence suggests that this type of reaction may be an important producer of fine-grained matrix plagioclase.

Recrystallized plagioclase in myrmekite-like intergrowths with quartz is substantially more calcic (X_{Ca} = 0.56 – 0.82) than the replaced plagioclase grain (X_{Ca} = 0.38-0.44; Fig. 37b), or any other plagioclase analysed in the sheared or unsheared tonalite. This microstructure is only observed in a thin (~1 cm) band in one of the strongly sheared samples (C), and may result from preferential leaching of Na during fluid fluxing or local Ca enrichment resulting from hornblende breakdown.

Figure 37. Backscattered electron image showing symplectic plagioclase, biotite and titanite replacing primary biotite.

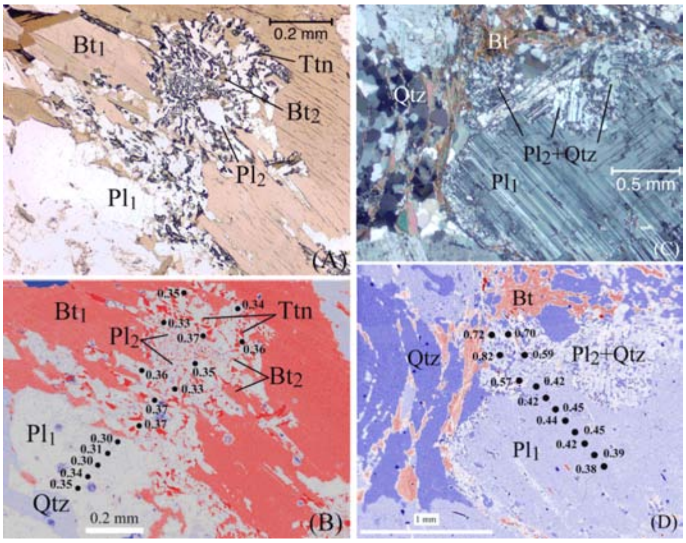

(A) Photomicrograph and (B) backscattered electron image showing symplectic intergrowths of fine-grained plagioclase (Pl_2), biotite (Bt_2) and titanite (Ttn) replacing a primary igneous biotite grain (Bt_1). Points on backscatter image show plagioclase anorthite content. Photomicrograph plane-polarized light. (C) Photomicrograph and (D) backscattered electron image showing symplectic intergrowths of fine-grained plagioclase (Pl_2) and quartz (Qtz) replacing a primary igneous plagioclase grain (Pl_1). Points on backscatter image show plagioclase anorthite content. Photomicrograph crossed polars.

4.2.2. Biotite

As with plagioclase, systematic changes in biotite composition occur from the pluton interior into the shear zone. The biotite in the less deformed rocks is typically greenish brown, but much of the biotite that forms incipient new foliae in these rocks is red-brown. The red-brown biotite becomes more abundant with increased deformation and the biotite in the higher strain rocks is all red-brown. These observations suggest that the reactions responsible for the abundance of red-brown biotite in the mylonites were incipient in the least deformed rocks.

The most notable chemical difference accompanying this color change is a progressive increase in Al and decrease in Fe in biotite from higher strain rocks (Fig. 35; Table 3). The compositional changes coincide with syn-deformational production of new biotite grains through recrystallization of primary biotite grains, precipitation of fine-grained biotite in strain shadows adjacent to plagioclase clasts, and the replacement of hornblende by biotite via an inferred local reaction represented by the generalized equation:

$$Hbl + K + H_2O = Bt_2 + Ca$$

We infer that the additional H_2O and K needed to drive this reaction were provided primarily by infiltration of fluids through the shear zone, with some additional K available through the replacement of minor igneous K-feldspar by myrmekite. Depletion of Fe in the new biotite is consistent with the bulk decrease in Fe within the shear zone, whereas the Al enrichment could be due to its apparent immobility during metasomatism.

4.2.3. Hornblende

Magmatic hornblende is present throughout the Cerro de Costilla complex tonalite, but is conspicuously absent from the strongly sheared samples (A-C). This is presumably due to hornblende breakdown to biotite (Eq. 2). Primary hornblende grains fall within the edenite to magnesio-hornblende compositional range and commonly have moderate compositional zoning, with increasing Ca concentrations from core to rim. The hornblende mode is consistent across the tonalite interior, although the chemical composition changes. In sample D, fine-grained blue-green actinolitic hornblende is observed in the matrix foliation and on the margins of fragments. Lower Na, K, Fe, Ti, and Al, and higher Mg and Si concentrations are observed in both new (blue-green) and primary hornblende grains in sample D relative to H. These compositional changes are consistent with Fe-Mg exchange and the edenite substitution (exchange vector = $Na_{-1}Al_{-1}Si$; Thompson *et al.*, 1982), which describes the solid solution between Na and Al-rich edenite and actinolite. The compositional change could reflect re-equilibration at the lower crustal temperatures that occurred during deformation, as suggested by lower Ti concentrations (Otten, 1984, Pattison, 2003) or changes in the local effective bulk composition related to metasomatic mass exchange.

4.3. Hornblende – plagioclase thermometry

The compositions of coexisting hornblende and plagioclase grains within the foliated matrix of sample D were used to estimate the temperature of deformation (Table 4). Temperature estimates were calculated for various pressures using the hornblende-plagioclase thermometer of Holland and Blundy (1994), which is based on the edenite exchange equilibrium: Ed + 4Qtz = Tr + Ab. This thermometer was selected because of the observed change from primary edenitic hornblende to recrystallized actinolitic hornblende (*e.g.*, Figs 20 and 21a) through edenite component exchange, the abundance of quartz in all samples (*i.e.*, silica saturation), and its calibration down to 400°C. At 3 kbar, the calculated temperatures range from 490°C to 576°C, with an average of 538°C. Owing to the possibility of incomplete equilibration between each grain pair and the minor pressure dependence of the calculated values, we adopt a conservative uncertainty of + 75°C. It is possible that shearing in the hornblende-free marginal samples (A-C) continued during cooling, and therefore we consider ~540 + 75°C an upper limit on shear-zone temperature during deformation. This is consistent with the microstructural evidence, and in view of all evidence and data, we suggest that a reasonable bracket for the deformation temperature is 475 ± 50°C.

Figure . Table 4.

	Matrix Hbl-Pl						
Pair	1	2	3	4	5	Avg	S.D.
Parameter							
XSi,T1	0.83	0.80	0.77	0.85	0.86	0.8	0.0
XAl,T1	0.17	0.20	0.23	0.15	0.14	0.2	0.0
XAl,M2	0.22	0.24	0.28	0.20	0.21	0.2	0.0
Xvac,A	0.90	0.85	0.84	0.90	0.93	0.9	0.0
XNa,A	0.05	0.08	0.09	0.05	0.03	0.1	0.0
XNa,M4	0.05	0.06	0.06	0.04	0.04	0.1	0.0
XCa,M4	0.91	0.92	0.91	0.93	0.91	0.9	0.0
XK,A	0.05	0.07	0.07	0.05	0.04	0.1	0.0
Ked-tr	6.00	3.02	2.09	6.52	12.26	6.0	4.0
T °C (3 kbar)	**528.7**	**561.3**	**576.0**	**530.9**	**490.5**	**537.5**	**33.1**

Parameters and calculated temperatures for Hornblende-Plagioclase pairs used for thermometry (after Holland and Blundy, 1994).

5. Discussion

5.1. Origin of 'beard' structures

The quartz-biotite 'beards' described previously appear to be unusual in mylonites, where smaller 'tails' or 'wings' attached to well separated porphyroclasts in an abundant, fine-grained matrix are more common. In the Cerro de Costilla rocks, the abundance of large plagioclase clasts may have controlled the development of 'beards' by protecting lower-strain zones between the clasts, attracting components in solution, and promoting nucleation of quartz and mica on the plagioclase. We interpret the beards as indicating solution of biotite and quartz components in high-mean stress or high-strain sites and transport of components in solution to low-mean stress sites, where they nucleate as minerals on the plagioclase clasts, the mineral alignment defining the stretching direction.

Beards are common on clasts in low-grade deformed rocks, such as slates (*e.g.*, McClay, 1977; Powell, 1982; Cox and Etheridge, 1982, 1983; Gray and Wright, 1984; Waldron and Sandiford, 1988; Gray and Willman, 1991; Vernon, 2004). For example, quartz-white mica 'beards' between quartz clasts in deformed quartz-rich sandstone have been illustrated by Dunlap and Teyssier (1998, fig. 86B). They have also been described in high-grade mylonitic rocks. For example, Lafrance and Vernon (1993, 1998) described hornblende beards on former pyroxene grains in mylonitic metagabbro, and Wintsch and Yi (2002) described beard structures in granodioritic orthogneiss. A variation on this theme is provided by oriented symplectites of orthopyroxene and plagioclase on garnet in mafic mylonites described by Brodie (1995, 1998). In both these gabbroic examples, growth of the beards was associated with breakdown and partial replacement of the clasts on which the beards were growing.

Creep by dissolution and precipitation may occur at high temperatures during deformation in the presence of water, as noted by Lafrance and Vernon (1993, 1999) for gabbro deformed at high-temperature amphibolite facies conditions, and by Wintsch and Yi (2002) for granodioritic orthogneiss deformed at 500-600°C. Lafrance and Vernon (1993, 1999) inferred that plagioclase flowed by dislocation creep and recrystallized, but that pyroxene and hornblende mainly fractured and developed fringes of aligned grains (beard structures) between boudins. Wintsch and Yi (2002) inferred that, though biotite and quartz deformed by dislocation creep, most of the deformation was accomplished by deformation-enhanced dissolution of minerals at grain boundaries perpendicular to the shortening direction — indicated by truncated zoning patterns in plagioclase, orthoclase, epidote and titanite — and precipitation in the form of beards on the ends of grains that faced the extension direction. Both of these examples show that solution-precipitation creep can accompany and even dominate over dislocation creep at high temperatures in the presence of water.

5.2. Metasomatic alteration

The modal and chemical changes across the shear zone suggest that fluid-rock interaction and mass transfer occurred synchronously with deformation (*e.g.*, Lonka et al, 1998; Barnes *et al.*, 2004; O'Hara, 2007). In this section, the geochemical data described above are used to estimate the amount of fluid that may have been involved and explore the possibility of fluid-enhanced chemical mixing between the marginal Cerro de Costilla and the host rocks.

5.2.1. Fluid-rock ratios

The volume of externally-derived fluid that interacted with the shear zone rock is estimated through the calculation of fluid-rock ratios. The calculations are based on an inferred increase in bulk SiO_2 during metasomatic alteration (Table 1) relative to the designated immobile species (Al_2O_3, TiO_2, and Zr). Fluid-rock ratios (N) were calculated from average SiO_2, Al_2O_3, TiO_2, and Zr whole-rock concentrations (C) using the equation:

$$N = \frac{\left(C_{Si^a}\left[\frac{C_{Al^a}}{C_{Al^o}}\right] - C_{Si^o}\right)}{C_{Si^f}(l-s)}$$

(after O'Hara & Blackburn, 1989), where a = altered samples (B and C), o = protolith samples (D-J), C_{Si}^{f} = SiO_2 solubility in the fluid, and s = SiO_2 saturation in the fluid,. N was calculated for silica saturation values of 0%, 25%, 50%, 75%, and 95%, and a SiO_2 solubility of 3g/kg was assumed, in accordance with the approximate temperature of deformation (Fournier & Potter, 1982). Ratios calculated using the Al_2O_3, TiO_2 and Zr reference frames are all nearly identical, namely 0.25-6.0 for SiO_2 saturations between 0%-95% (Table 5). The presence of recrystallized quartz-rich pods and strain shadows in sheared marginal rocks suggests that SiO_2 saturation may have approached 100% (at least locally), and thus actual fluid-rock ratios may be closer to the high end of the above range (approximately 6.0).

Figure . Table 5.

% Saturation	0	25	50	75	95
Fluid:Rock					
Si-Al	0.30	0.40	0.60	1.20	5.99
Si-Ti	0.24	0.32	0.48	0.96	4.79
Si-Zr	0.27	0.37	0.55	1.10	5.50

Fluid-rock ratios calculated from bulk geochemical changes (after O'Hara and Blackburn, 1989).

5.2.2. Two-component mixing model

To determine whether the bulk compositional changes observed in samples A-C could have resulted from chemical exchange with the host granitic gneisses (*i.e.*, local mass transfer), two-component mixing models were constructed from bulk chemical data using groups of three elements X, Y, and Z in the form of binary plots of X/Y vs Z (after Yang *et al.*, 1998). The hyperbolic mixing curves between end-member compositions have the general form:

$$\left(\frac{X}{Y}\right)_m = \frac{a}{Z_m} + b$$

where m denotes the mixed composition of interest, and a and b are obtained from the tonalitic protolith (P) and host rock (H) end-member compositions, such that:

$$a = \frac{Z_p Z_h \left[\left(\frac{X}{Y}\right)_H - \left(\frac{X}{Y}\right)_P\right]}{(Z_P - Z_H)}$$

$$b = \frac{Z_P \left(\frac{X}{Y}\right)_P - Z_H \left(\frac{X}{Y}\right)_H}{(Z_P - Z_H)}$$

Major and trace element concentrations of the average interior tonalite samples (D-J; protolith) and from published chemical data on granitic orthogneisses (host rock) from the Pine Valley Suite of the Peninsular Ranges batholith (Todd *et al.*, 2003) were used in the calculations (Table 1).

Mixing curves calculated for the "mobile" major elements generally show close agreement with the observed concentrations in the marginal samples. The observed concentrations of SiO_2, K_2O, CaO, Fe_2O_3, and MgO in marginal samples B and C plot close to the curves predicted for a two-component mixture (Fig. 38). Na_2O concentrations in the marginal samples are much lower than in both the unaltered tonalite and host gneisses, and thus a bulk leaching of Na_2O from the sheared margin is suggested. Overall, most major element concentrations in the marginal Cerro de Costilla are consistent with fluid-assisted mixing of chemical components from the tonalite protolith with those of the adjacent host rocks during deformation, although alternative explanations cannot be ruled out.

Figure 38. Two component mixing model for undeformed Cerro de Costilla tonalite and host granitic orthogneiss.

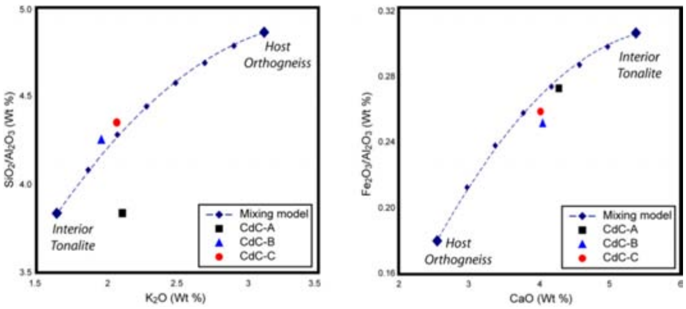

Two component mixing model for undeformed Cerro de Costilla tonalite and host granitic orthogneiss. Concentrations of mobile elements SiO_2, K_2O, CaO, and Fe_2O_3 within the sheared margin plot close to the theoretical mixing model curves calculated for the undeformed tonalite and host orthogneiss end members.

5.3. Coupling of mechanical and chemical processes in strain localization

Microstructural observations, combined with chemical data indicate that the coupling of mechanical and chemical processes played an important role in the development of mylonitic fabric evolution and modal changes in the shear zone. The occurrence of small new grains of biotite and fragmental plagioclase along grain boundaries and fracture surfaces indicates that fracturing and dilatancy of the plagioclase framework enabled localized fluid access and grain growth along the newly exposed surfaces (*e.g.* Fitz Gerald & Stünitz, 1993, Collettini & Holdsworth, 2004; Marsh *et al.*, in press). With increasing strain, the main physical and chemical processes involved in the fabric evolution were: (1) fragmentation and cleavage slip of biotite, (2) recrystallization and dislocation creep of quartz, (3) fragmentation and granular flow of plagioclase, hornblende, titanite and rare epidote, (4) replacement of hornblende by biotite, (5) solution/re-precipitation of biotite and quartz, (6) replacement of rare K-feldspar by myrmekitic intergrowths, followed by recrystallization and dislocation creep of these aggregates, and (7) replacement of biotite by symplectic titanite-plagioclase intergrowths, followed by fragmentation and/or recrystallization and dislocation creep and/or granular flow of these aggregates.

As continuous biotite-rich foliae developed, and fine-grained quartz and biotite precipitated behind plagioclase grains to form 'beards', the increased interconnectivity of the fine-grained matrix enhanced the effective permeability of the rocks, allowing faster diffusion/advection rates (*e.g.* Carlson & Gordon, 2004) through an intergranular fluid phase. In the most highly strained rocks (samples A-C), strain appears to have been increasingly accommodated by dissolution-precipitation creep, as evidenced by synkinematic precipitation of biotite and quartz, although dislocation creep remained active in quartz. The development of a sharp microstructural and mineralogical front between samples C and D suggests strong coupling among fluid, reaction and strain in the most highly deformed rocks (samples A-C). We infer that the development of a continuous foliation and reduced grain size with proximity to the pluton margin enhanced effective permeability, and thus enabled the efficient fluid mobility and element exchange required for the reactions to proceed. In this narrow (1-m) zone, reaction rates may have increased sufficiently to keep up with bulk strain-rates (*e.g.* Baxter & DePaolo, 2004; O'Hara, 2007).

A conceptual illustration of fluid-chemical-mechanical coupling is shown in Fig. 39. In this framework, deformation is described through the velocity gradient tensor, effective viscosity being the controlling physical parameter. Intergranular mass transport is described by diffusion and fluid advection. Reactions are described through a rate equation. Various interactions, or couplings, are illustrated among the three principal processes. Coupling of deformation and reaction is manifest by hardening or softening of rock as a function of mineralogical change, and is thus the simplest representation of interaction between the velocity field and rheological evolution. This coupling also facilitates strain-sensitive reaction in which deformation increases the number of paths for reaction progress. Coupling of deformation and diffusion can arise through diffusion and/or advection terms. Note that the diffusion, advection, reaction equation treats the full velocity field around a point, so that deformation is also expressed through an advection term. Stretching and folding of material due to deformation changes diffusion lengths and fluid pathways, which can serve to reduce or eliminate the time-dependent decay of chemical potential gradients (*e.g.*, Ottino, 1989). Deformation also changes the microstructure, typically leading to grainsize reduction and more efficient grain-boundary transport paths. Coupling between diffusion/fluid advection and reaction rate can be expressed, for example, through the evolution of porosity and the spatial dependence of thermodynamic affinity.

Figure 39. Coupling of deformation, reaction and diffusion/advection in the transformation of tonalite to mylonite.

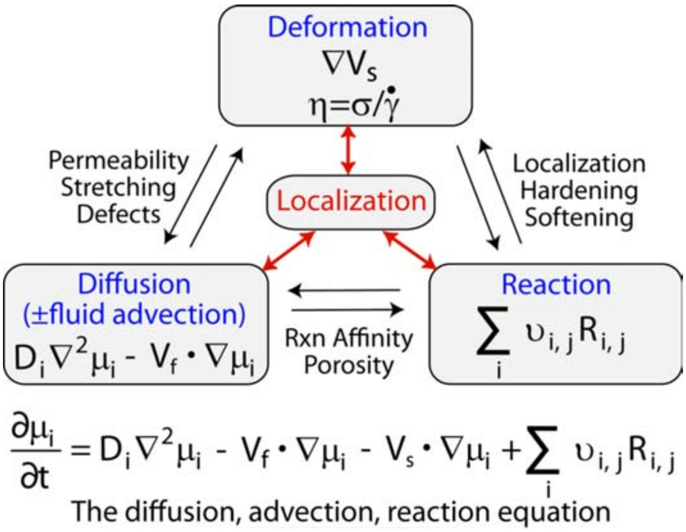

Transformation of tonalite to mylonite framed as a three-way coupling among deformation, diffusion/advection, and reaction. ∇ = the gradient operator, V = velocity, η = viscosity, σ = shear stress, γ = shear strain rate, D = diffusion constant, = chemical potential, υ = stoichiometric coefficient, R = rate of production or depletion, subscript i = species, subscript j = reaction, subscript f = fluid and subscript s = solid. Important limiting assumptions in the diffusion, advection, reaction equation include: (1) D_i is spatially constant, and (2) transport processes and chemical reactions do not affect the mechanics. Modifications to the equation can reflect changes in the mechanics, as defined by changes in rheology, with time.

5.4. Rheological effects

In the Cerro de Costilla, coupled microstructural and chemical processes led to strain-dependent weakening and strain localization mainly by: (1) the progressive breakdown by fracturing, fragmentation and reaction of the load-bearing plagioclase framework; (2) the progressive development of continuous biotite-rich foliae; (3) flow of quartz into lenticular foliae once the restricting plagioclase framework had sufficiently broken down; (4) elimination of strong hornblende accompanied by modal increase of weaker biotite; (5) dissolution, transport and re-deposition of biotite and quartz components in lower shear-strain sites between zones of continuous biotite-rich foliae; (6) overall grain-size reduction through fragmentation, recrystallization and neocrystallization of the main minerals; and (7) minor contributions from fine-grained aggregates of other minerals.

The end result of these processes is the development of a fully interconnected weak matrix studded with isolated plagioclase porphyroclasts. This type has been referred to as an interconnected weak phase (IWP; Handy, 1990) or weak phase supported (WPS; Ji *et al.*, 2001; Takeda and Griera, 2006) microstructure, and has been shown to approach an iso-stress state (Reuss model) and a strength minimum (Ji, 2004; Takeda and Griera, 2006). The strength of the rock should therefore approach the strength of the dominant interconnected matrix mineral, which in this case is biotite. Micas are known to be among the weakest minerals in shear along their (001) planes at upper greenschist to lower amphibolite facies conditions, which are consistent with mylonite development in the Cerro de Costilla rocks (*e.g.*, Kronenberg *et al.*, 1990; Tullis and Wenk, 1994; Niemeijer and Spiers, 2005). Recent numerical (Johnson *et al.*, 2004) and laboratory (Holyoke and Tullis, 2006; Mariani *et al.*, 2006) experiments provide some guidance on how much weakening could be expected during the development of the most highly strained rocks studied here.

Johnson *et al.* (2004) combined detailed microstructural analysis of a preserved strain gradient within the sheared margin of the San Jose pluton in Baja California, México with grain-scale numerical modelling to explore the rheological effects of progressive coalescence of weak minerals. Johnson *et al.* (2004) showed that deformation was initiated by localized fracturing of the plagioclase framework near the tips of isolated biotite grains – as described here and by Marsh *et al.* (in press). Progressive development of continuous foliae occurred almost entirely by mechanical processes, leading to a mylonitic foliation in the most highly strained rocks at the pluton margin. Johnson *et al.* (2004) conducted numerical experiments to evaluate the initiation of these shear zones. With a starting geometry based on the least deformed portions of the pluton and general shear boundary conditions, localized zones of high differential stress and shear-strain rate developed in the “plagioclase” matrix adjacent to the tips of weak “biotite” grains. The localized zones of high differential stress reached values up to 2 times the confining pressure, leading to failure of the matrix and initiation of microshear zones. With continued deformation, elongate high strain-rate zones linking weak “biotite” grains developed across “plagioclase” bridges, these zones accommodating shear strain rates up to 2.5 orders of magnitude greater than in the adjacent matrix.

Similar results were obtained by Holyoke and Tullis (2006a, b), who conducted triaxial shear experiments on fine-grained quartzofeldspathic gneiss containing approximately 13 vol. % biotite. At the early stages of deformation, slip on biotite (001) planes caused microfaulting in quartz grains separating biotite grains. With continued strain, biotite interconnection occurred by localized semi-brittle flow of the quartz. At higher shear strains ($\gamma \approx 3$), through-going biotite-bearing microshear zones developed, coincident with a maximum stress drop of approximately 40%. At this advanced stage, shear strain rates within the microshear zones were approximately two orders of magnitude greater than in the adjacent rock, as found in the modelling of Johnson *et al.* (2004).

Mariani *et al.* (2006) conducted triaxial shear experiments designed to investigate the shear strength of continuous muscovite foliae in faults and shear zones. They used wet pressed polycrystalline muscovite layers with {001} planes at 45° to the loading axis, and pore water pressures of approximately 100 MPa to inhibit dehydration reactions in experimental runs spanning temperatures of 400 to 700°C. At relatively low strain rates and high temperatures, they observed marked strength drops, and the mechanical results suggest linear viscous creep. Mariani *et al.* (2006) concluded that mica-rich rocks may flow at shear stresses as low as 1-10 MPa at strain rates of 10^{-13} s^{-1} and temperatures consistent with upper greenschist to lower amphibolite facies metamorphism.

Given the results of these three studies, it is possible that the strength of the Cerro de Costilla rocks dropped from the frictional strength of plagioclase at approximately 10 km depth under hydrostatic fluid pressure conditions in a subvertical extensional fault to perhaps 10 MPa or lower. Such a strength drop would be close to an order of magnitude, but the lower bound is constrained by viscous basal creep in mica. Given that strain in the most deformed shear-zone samples was accommodated also (maybe largely) by dissolution/precipitation processes, we speculate that coupling of deformation, diffusion, fluid advection and reaction in the wet core of the mylonite zone may have allowed strain to accumulate at even lower shear stresses.

6. Conclusions

Progressive deformation of hornblende-biotite tonalite of the Cerro de Costilla complex (Baja California, México) in a mylonitic shear zone involved cleavage slip in biotite to initiate discontinuous foliae, which became linked via fine-grained aggregates involving fragmental and recrystallized biotite, recrystallized quartz, fine-grained plagioclase and titanite after biotite, fragmental plagioclase, minor fragmental hornblende and recrystallized myrmekite, to form more continuous foliae anastomosing around resistant plagioclase framework grains. At an intermediate stage of fabric development, continuous foliae were localized around plagioclase grain boundaries forming a distinct S/C-type pattern. Although the C-surfaces are parallel to the shear-zone boundary, the S-surface are controlled by the orientations of plagioclase grain boundaries (*e.g.*, Passchier and Simpson, 1986), and so do not represent a progressively rotating foliation that marks the direction of maximum finite elongation, as in the original S/C terminology (Berthé *et al.*, 1979).

The amount of strain accumulation increases markedly close to the contact between the tonalite and the wall-rock orthogneiss, where hornblende disappears in favor of biotite, and continued deformation has resulted in elongation of recrystallized quartz aggregates to form lenticular ribbon-like foliae, as well as the development of biotite-quartz-plagioclase 'beards' on resistant plagioclase clasts. Increasing separation of the clasts and consequent extension and recrystallization of the beards produced a fine-grained foliated matrix between the clasts. This was accompanied by collapse of biotite foliae into the inter-clast sites, resulting in partial loss of the S/C structure in favor of a more symmetrical anastomosing foliation. Extensive recrystallization of the matrix produced fine-grained decussate aggregates of biotite and aggregates of quartz and biotite with low-energy grain shapes.

The deformation occurred at approximately 475 ± 50°C, which was too low for extensive plagioclase recrystallization, and was accompanied and assisted by chemical reactions, such as: (1) replacement of biotite by symplectic plagioclase and titanite and by replacement of minor interstitial K-feldspar by myrmekite, these fine-grained aggregates recrystallizing readily to provide fine-grained granular aggregates capable of contributing to foliation initiation and development; (2) replacement of hornblende by biotite, which provided a higher proportion of weaker material; and (3) transport of biotite and quartz components in solution to sites of low compressive stress and shear strain in the lee of plagioclase porphyroclasts.

Coupling of deformation, diffusion, fluid advection and reaction in the wet core of the mylonite zone led to a strong fabric and strain gradient over a very short distance (approximately 50 cm) between samples D and C. The loss of hornblende across the transition, coupled with an increase in modal biotite and quartz, and enhanced dissolution-precipitation accommodated strain led to weakening and localization. The overall contributing factors in weakening were: (1) the progressive breakdown by fracturing, fragmentation and reaction of the load-bearing plagioclase framework; (2) the progressive development of continuous biotite-rich foliae; (3) flow of quartz into lenticular foliae, once the restricting plagioclase framework had sufficiently broken down; (4) elimination of strong hornblende accompanied by modal increase of weaker biotite; (5) dissolution, transport and re-deposition of biotite and quartz components in lower shear-strain sites between zones of continuous biotite-rich foliae; and (6) minor contributions from fine-grained aggregates of other minerals.

Acknowledgements

We acknowledge support from National Science Foundation grants EAR-0440063 and EAR-0810039 (to Johnson) and a University of Maine Doctoral Research Fellowship (to Marsh). We thank Erwin A. Melis for helping to collect the samples used in this study.

References

Ague, J. J. 1994: Mass transfer during Barrovian metamorphism of pelites, south-central Connecticut. I: Evidence for changes in composition and volume. American Journal of Science, 294, 989-1057.

Barnes, J. D., Selverstone, J. & Sharp, Z. D. 2004. Interactions between serpentine devolatilization, metasomatism and strike-slip strain localization during deep-crustal shearing in the Eastern Alps. Journal of Metamorphic Geology, 22, 283-300.

Baumgartner, L. P. & Olsen, S. N., 1995. A least-squares approach to mass transport calculations using the Isocon method. Economic Geology, 90, 1261-1270.

Baxter, E. F. & DePaolo, D. J., 2004. Can metamorphic reactions proceed faster than bulk strain? Contributions to Mineralogy and Petrology, 146, 657-670.

Bell, T. H. & Etheridge, M. A. 1973: Microstructure of mylonites and their descriptive terminology. Lithos, 6, 337-348.

Berthé, D., Choukroune, P. & Jegouzo, P. 1979: Orthogneiss, mylonite and non-coaxial deformation of granites: the example from the South Amorican shear zone. Journal of Structural Geology, 1, 31-42.

Bons, P.D., Cox, S.J.D., 1994. Analogue experiments and numerical modeling on the relation between microgeometry and flow properties of polyphase materials. Materials Science and Engineering, A175, 237-245.

Bons, P.D., Urai, J.L., 1994. Experimental deformation of two-phase rock analogues. Materials Science and Engineering, A175, 221-229.

Bons, P.D., Jessell, M.W., 1999. Micro-shear zones in experimentally deformed octachloropropane. Journal of Structural Geology, 21, 323-334.

Bos, B. & Spiers, C. J., 2001. Experimental investigation into the microstructural and mechanical evolution of phyllosilicates-bearing fault rock under conditions favoring pressure solution. Journal of Structural Geology, 23, 1187-1202.

Brodie, K.H., 1995. The development of orientated symplectites during deformation. Journal of Metamorphic Geology 13, 499-508.

Brodie, K.H., 1995. High-temperature mylonites: 1. Metabasic mylonites. In: Snoke, A.W., Tullis, J., Todd, V.R. (eds): Fault-related Rocks: a Photographic Atlas. Princeton University Press, Princeton, 428-435.

Carlson, W. D. & Gordon, C. L., 2004. Effects of matrix grain size on the kinetics of intergranular diffusion. Journal of Metamorphic Geology, 22, 733-742.

Christiansen, P.P., Pollard, D.D., 1997. Nucleation, growth and structural development of mylonitic shear zones in granitic rock. Journal of Structural Geology, 19, 1159-1172.

Collettini, C., & Holdsworth, R. E., 2004. Fault zone weakening and character of slip along lowangle normal faults: insights from the Zuccale fault, Elba, Italy. Journal of the Geological Society, 161, 1039-1051.

Connolly, J.A.D., Holness, M.B., Rubie, D.C., Rushmer, T., 1997. Reaction-induced microcracking; an experimental investigation of a mechanism for enhancing anatectic melt extraction. Geology 25, 591–594.

Cox, S.F., Etheridge, M.A., 1982. Fiber development in deformed hydrothermally altered acid volcanic rock. In: Borradaile, G.J., Bayly, M.B., Powell, C.M. (eds): Atlas of Deformational and Metamorphic Rock Fabrics. Springer, New York, 304-305.

Cox, S.F., Etheridge, M.A., 1983. Crack-seal fibre growth mechanisms and their significance in the development of oriented layer silicate microstructures. Tectonophysics 92, 147-170.

Davidson, C., Schmid, S.M., Hollister, L.S., 1994. Role of melt during deformation in the deep crust. Terra Nova 6 (2), 133–142.

Drury, M.R., Vissers, R.L.M., van der Wal, D., Hoorgerduin Strating E.H., 1991. Shear localization in upper mantle peridotites. Pure and Applied Geophysics, 137, 439-460.

Dunlap, W.J., Teyssier, C., 1998. Dating deformation in mylonites. In: Snoke, A.W., Tullis, J., Todd, V.R. (eds):Fault-related Rocks. A Photographic Atlas. Princeton University Press, Princeton, p. 282.

Faulkner, D.R., Lewis, A.C., Rutter, E.H., 2003. On the internal structure and mechanics of large strike-slip fault zones: field observations of the Carboneras fault in southeastern Spain. Tectonophysics 367, 235-251.

Fitz Gerald, J.G., Stünitz, H., 1993. Deformation of granitoids at low metamorphic grade. I: Reactions and grain size reduction. Tectonophysics 221, 269-297.

Fournier, R. O. & Potter, R. W., 1982. An equation correlating the solubility of quartz in water from 25° to 900° C at pressures up to 10,000 bars. Geochemica et Cosmochemica Acta, 46, 1969-1973.

Gapais, D. 1989: Shear structures within deformed granites: Mechanical and thermal indicators. Geology, 17, 1144-1147.

Gastil, R.G., Phillips, R.P., Allison, E.C., 1975. Reconnaissance geology of the State of Baja California. Geological Society of America Memoir 140, 170 p.

Goodwin, L. B., Wenk, H.-R. 1995: Development of phyllonite from granodiorite: mechanisms of grain-size reduction in the Santa Rosa mylonite zone, California. Journal of Structural Geology, 17, 689-707.

Gottschalk, R.R., Kronenberg, A.K., Russell, J.E., Handin, J., 1990. Mechanical Anisotropy of gneiss: Failure criterion and textural sources of directional behavior. Journal of Geophysical Research, 95, 21613-21634.

Grant, J. A., 1986. The Isocon diagram-A simple solution to Gresens' equation for metasomatic alteration. Economic Geology, 81, 1976-1982.

Grant, J. A., 2005. Isocon analysis: A brief review of the method and applications.. Physics and Chemistry of the Earth, 30, 997-1004.

Gray, D.R., Willman, C.E., 1991. Thrust-related strain gradients and thrusting mechanisms in a chevron-folded sequence, southeastern Australia. Journal of Structural Geology 13, 691-710.

Gray, D.R., Wright, T.O., 1984. Problems of volume loss, fabric development, and strain determination in low-grade pelitic rocks, Martinsburg Formation, U.S.A. Journal of Structural Geology 7, 492.

Handy, M.R., 1989. Deformation regimes and the rheological evolution of fault zones in the lithosphere: the effects of pressure, temperature, grain size and time. Tectonophysics 163, 119-152.

Handy, M.R., 1990. The solid-state flow of polymineralic rocks. Journal of Geophysical Research, 95, 8647-8661.

Handy, M.R., 1994. The energetics of steady state heterogeneous shear in mylonitic rock. Materials Science and Engineering, A175, 261-272.

Handy, M.R., Wissing, S.B., Streit, L.E., 1999. Frictional-viscous flow in mylonite with varied bimineralic composition and its effect on lithospheric strength. Tectonophysics, 303, 175-191.

Handy, M.R., Mulch, A., Rosenau, M., Rosenberg, C.L., 2001. The role of fault zones and melts as agents of weakening, hardening and differentiation of the continental crust: a synthesis. In: R.E. Holdsworth, R.A. Strachan, J.F. Magloughlin, R.J. Knipe (eds),, The nature and tectonic significance of fault zone weakening. Geological Society, London, Special Publication 186, 305-332.

Handy, M.R., Hirth, G., R. Bürgmann, 2007. Continental fault structure and rheology from the frictional-to-viscous transition downward. In: M.R. Handy, G. Hirth, N. Hovius (eds): Tectonic Faults - Agents of Change on a Dynamic Earth, Dahlem Workshop Report 95, The MIT Press, Cambridge, Mass., USA, pp. 139-181.

Hirth, G., Tullis, J. 1992. Dislocation creep regimes in quartz aggregates. Journal of Structural Geology 14, 145-160.

Holland, T. & Blundy, J. 1994. Non-ideal interactions in calcic amphiboles and their bearing on amphibole-plagioclase thermometry. Contributions to Mineralogy and Petrology, 116, 433-447.

Holyoke, C.W. III, Rushmer, T., 2002. An experimental study of grain scale melt segregation mechanisms in two common crustal rock types. Journal of Metamorphic Geology 20, 493–512.

Holyoke, C. W. & Tullis, J., 2006a. The interaction between reaction and deformation: an experimental study using a biotite + plagioclase + quartz gneiss. Journal of Metamorphic Geology, 24, 743-762.

Holyoke, C. W. & Tullis, J., 2006b. Formation and maintenance of shear zones. Geology, 34, 105-108.

Imber, J., Holdsworth, R.E., Butler, C.A., Strachan, R.A., 2001. A reappraisal of the sibson–scholz fault zone model: the nature of the frictional to viscous (“brittle–ductile”) transition along a longlived, longlived, crustal–scal fault, Outer Hebrides, Scotland. Tectonics 20 (5), 601–624.

Ji, S. 2004. A generalized mixture rule for estimating the viscosity of solid-liquid suspensions and mechanical properties of polyphase rocks and composite materials. Journal of Geophysical Research, 109, doi: 10.1029/2004/JB003124

Ji, S., Wang, Z. and Wirth, R. 2001. Bulk flow strength of forsterite-enstatite composites as a function of forsterite content. Tectonophysics 341, 69-93

Jin, D., Karato, S., Obata, M., 1989. Mechanisms of shear localization in the continental lithosphere: interence from the deformation microstructures of peridotites from the Ivrea zone, northern Italy. Journal of Structural Geology, 20, 195-209.

Johnson, S.E., Tate, M.C. and Fanning, C.M., 1999. New geological and SHRIMP U-Pb zircon data in the Peninsular Ranges batholith, Baja California, México: Evidence for a suture? Geology, 27, 743-746.

Johnson, S.E., Schmidt, K.L. and Tate, M.C., 2002. Ring complexes in the Peninsular Ranges Batholith, Baja California, México and southern California, USA: middle- to upper-crustal magma plumbing systems. Lithos, 61, 187-208.

Johnson, S.E., Fletcher, J.M., Fanning, C.M., Vernon, R.H., Paterson, S.R. Tate, M.C., 2003. Structure, emplacement and lateral expansion of the San José tonalite pluton, Peninsular Ranges batholith, Baja California, México. Journal of Structural Geology, 25, 1933-1957.

Johnson, S. E., Vernon, R. H., Upton, P., 2004. Foliation development and progressive strain-rate partitioning in the crystallizing carapace of a tonalite pluton: microstructural evidence and numerical modeling. Journal of Structural Geology 26, 1845-1865.

Jordan, P., 1987. The deformational behaviour of bimineralic limestone – halite aggregates. Tectonophysics, 135, 185-197.

Jordan, P., 1988. The rheology of polymineralic rocks - an approach. Geologische Rundschau, 77, 285-294.

Kronenberg, A.K., Kirby, S.H., Pinkston, J., 1990. Basal slip and mechanical anisotropy of biotite. Journal of Geophysical Research, 95, 19257-19278.

Kruhl, J.H., 1996. Prism- and basal-plane subgrain boundaries in quartz: a microstructural geobarometer. Journal of Metamorphic Geology 14, 581-589.

Kruhl, J.H., 1998. Prism- and basal-plane subgrain boundaries in quartz: a microstructural geobarometer: Reply. Journal of Metamorphic Geology 16, 142-146.

Lafrance, B., Vernon, R.H., 1993. Mass transfer and microfracturing in gabbroic mylonites of the Guadalupe Igneous Complex, California. In: Boland, J. N., Fitz Gerald, J. D. (eds): Defects and Processes in the Solid State: Geoscience Applications. The McLaren Volume. Elsevier, Amsterdam, 151-167.

Lafrance, B., Vernon, R.H. 1999. Coupled mass transfer and microfracturing in gabbroic mylonites. In: Snoke, A.W., Tullis, J., Todd, V.R. (eds): Fault-related Rocks: a Photographic Atlas. Princeton University Press, Princeton, 204-207.

LaTour, T. E., 1987. Geochemical model for the symplectic formation of myrmekite during amphibolite-grade progressive mylonitization of granite. Geological Society of America Abstracts with Programs, 9, 741.

Lonka, H., Schulmann, K & Venera Z., 1998. Ductile deformation of tonalite in the Suomusjarvi shear zone, south-western Finland. Journal of Structural Geology, 20, 783-798.

Mares, V.M., Kronenberg, A.K., 1993. Experimental deformation of muscovite. Journal of Structural Geology 15 (9–10), 1061–1075.

Mariani, E., Brodie, K.H., Rutter, E.H., 2006. Experimental deformation of muscovite shear zones at high temperatures under hydrothermal conditions and the strength of phyllosilicate-bearing faults in nature. Journal of Structural Geology, 28, 1569-1587.

Marsh, J.H., Johnson, S.E., Yates, M.G. & West, D.P. Jr., 2009. Coupling of deformation and reactions during shear zone development at the frictional-to-viscous transition. Journal of Metamorphic Geology , in press.

McClay, K. R., 1977. Pressure solution and Coble creep in rocks and minerals: a review. Journal of the Geological Society of London 134, 57-70.

McLelland, J., Morrison, J., Selleck, B., Cunningham, B., Olson, C. & Schmidt, K. 2002a: Hydrothermal alteration of late- to post-tectonic Lyon Mountain Granitic Gneiss, Adirondack Mountains, New York: Origin of quartz-sillimanite segregations, quartz-albite lithologies, and associated Kiruna-type low-Ti Fe-oxide deposits. Journal of Metamorphic Geology, 20, 175-190.

McLelland, J., Goldstein, A., Cunningham, B., Olson, C. & Orrell, S 2002b: Structural evolution of a quartz-sillimanite vein and nodule complex in a late- to post-tectonic leucogranite, Western Adirondack Highlands, New York. Journal of Structural Geology, 24, 1157-1170.

Melis, E.A., 2006. Structural, temporal and metamorphic evolution of the Main Mártir Thrust, Baja California, México. Unpublished Ph.D. thesis, University of Maine, 338 pp.

Montesi L.G.J., Hirth, G., 2003. Grain size evolution and the rheology of ductile shear zones: from laboratory experiments to postseismic creep. Earth and Planetary Science Letters 211, 97-110.

Niemeijer, A.R. and Spiers, C.J., 2005, Influence of phyllosilicates on fault strength in the brittle-ductile transition: Insights from rock analogue experiments In: High Strain Zones: Structure and Physical Properties, D. Bruhn and L. Burlini (eds) Special Publication. Geological Society of London, pp.303-327.

Oesterling, N., Heilbronner, R., Stünitz, H., Barnhoorn, A., Molli, G., 2007. Strain dependent variation of microstructure and texture in naturally deformed Carrara marble. Journal of Structural Geology, 29, 681-696.

O'Hara, K. D. & Blackburn, W. H., 1989. Volume-loss model for trace-element enrichments in mylonites. Geology, 17, 524-527

O'Hara, K. D., 2007. Coupled deformation and reaction softening processes: Retrograde shear zones in the Rosslare Complex, south-east Ireland. Irish Journal of Earth Sciences, 25, 63-80.

Otten, M. T., 1984. The origin of brown hornblende in the Artfjaellet gabbro and dolerites. Contributions to Mineralogy and Petrology. 86, 189-199.

Ottino, J.M., 1989, The kinematics of mixing : stretching, chaos, and transport, Cambridge University Press, New York, 364 p.

Passchier, C.W. and Simpson, C., 1986. Porphyroclast systems as kinematic indicators. Journal of Structural Geology, 8, 831-843.

Pattison, D. R. M., 2003. Petrogenetic significance of orthopyroxene-free garnet + clinopyroxene + plagioclase + quartz-bearing metabasites with respect to the amphibolite and granulite facies. Journal of Metamorphic Geology, 21, 21-34.

Powell, C.M., 1982. Overgrowths and mica beards on rounded quartz grains enclosed by cleavage folia. In: Borradaile, G.J., Bayly, M.B., Powell, C.M. (eds): Atlas of Deformational and Metamorphic Rock Fabrics. Springer, New York, 300-301.

Price, R.H., 1982. Effects of anhydrite and pressure on the mechanical behavior of synthetic rocksalt. Geophysical Research Letters, 9, 1029-1032.

Rawling, G.C., Baud, P., Wong, Teng-fong., 2002. Dilatency, brittle strength, and anisotropy of foliated rocks: Experimental deformation and micromechanical modeling. Journal of Geophysical Research, 107 (B10), 10.1029/2001JB000472.

Ree, J.-H, Kim, H.S., Han, R., Jung, H., 2005. Grain-size reduction of feldspars by fracturing and neocrystallization in a low-grade granitic mylonite and its rheological effect. Tectonophysics 407, 227-237.

Rosenberg, C. L., Stünitz, H., 2003. Deformation and recrystallization of plagioclase along a temperature gradient: an example from the Bergell tonalite. Journal of Structural Geology 25, 389-408.

Ross, J.V., Bauer, S.J., Hansen, F.D., 1987. Textural evolution of synthetic anhydrite–halite mylonites. Tectonophysics, 140, 307-326.

Segall, P. & Simpson, C. 1986: Nucleation of ductile shear zones on dilatant fractures. Geology 14, 56-59.

Shea, W.T. Jr., Kronenberg, A.K., 1992. Rheology and deformation mechanisms of an isotropic mica schist. Journal of Geophysical Research, 97, 15201-15237.

Shea, W.T. Jr., Kronenberg, A.K., 1993. Strength and anisotropy of foliated rocks with varied mica contents. Journal of Structural Geology, 15, 1097-1121.

Simpson, C., 1984. Borrego Springs¬Santa Rosa mylonite zone: a late Cretaceous west-directed thrust in southern California. Geology, 12, 8-11.

Simpson, C., 1985. Deformation of granitic rocks across the brittle¬ductile transition. Journal of Structural Geology, 7, 503-511.

Simpson, C. and Schmid, S.M., 1983. An evaluation of criteria to deduce the sense of movement in sheared rocks. Geological Society of America Bulletin, 94, 1281-1288.

Simpson, C. and Wintsch, R.P., 1989. Evidence for deformation-induced K-feldspar replacement by myrmekite. Journal of Metamorphic Geology 7, 261-275.

Stewart, M., Holdsworth, R.E., Strachan, R.A., 2000. Deformation processes and weakening mechanisms within the frictional-viscous transition zone of major crustal-scale faults: Insights from the Great Glen Fault Zone, Scotland. Journal of Structural Geology, 22, 543-560.

Stipp, M., Stünitz, H., Heilbronner, R., Schmid, S.M., 2002a. Dynamic recrystallization of quartz: correlation between natural and experimental conditions. In: de Meer, S., Drury, M.R., de Bresser, J.H., Pennock, G.M. (eds): Deformation mechanisms, Rheology and Tectonics: Current Sand Future Perspectives. Geological Society of London Special Publication 200, 171-190.

Stipp, M., Stünitz, H., Heilbronner, R., Schmid, S.M., 2002b. The eastern Tonale fault zone: a 'natural laboratory' for crystal plastic deformation of quartz over a temperature range from 250 to 700°C. Journal of Structural Geology 24, 1861-1884.

Taketa, Y.-T. and Griera, A., 2006, Rheological and kinematical response to flow of two-phase rocks. Tectonophysics, v. 427, p. 95-113.

Tharp, T.M., 1983. Analogies between the high-temperature deformation of polyphase rocks and the mechanical behavior of porous powder metal. Tectonophysics, 96, T1-T11.

Thompson, J. B., Laird, J. & Thompson, A. B. 1982. Reactions in Amphibolite, Greenschist and Blueschist. Journal of Petrology, 23, 1-27.

Todd, V.R., Shaw, S.E., Hammarstrom, J.M., 2003. Cretaceous plutons of the Peninsular Ranges batholiths, San Diego and westernmost Imperial Counties, California: Intrusion across a Late Jurassic continental matgin. In: Johnson, S.E., Paterson, S.R., Fletcher, J.M., Girty, G.H., Kimbrough, D.L., Martin-Barajas, A. (eds), Tectonic evolution of northwestern Mexico and the southwestern USA. Geological Society of America Special Paper 374, 185-235.

Tullis, J., Stünitz, H., Teyssier, C., Heilbronner, R., 2000. Deformation microstructures in quartzo-feldspathic rocks. In: Jessell, M.W., Urai, J.L. (eds): Stress, Strain and Structure. A Volume in Honour of W.D. Means. Journal of the Virtual Explorer 2 (print and CD).

Tullis, J., Wenk., H.-R., 1994. Effect of muscovite on the strength and lattice preferred orientations of experimentally deformed quartz aggregates. Materials Science and Engineering, A175, 209-220.

Tullis, J. & Yund, R. A. 1987: Transition from cataclastic flow to dislocation creep of feldspar: Mechanisms and microstructures. Geology, 15, 606-609.

Tullis, T.E., Horowitz, F.G., Tullis, J., 1991. Flow laws of polyphase aggregates from end-member flow laws. Journal of Geophysical Research, 96, 8081-8096.

Vernon, R.H., 1991. Questions about myrmekite in deformed rocks. Journal of Structural Geology 13, 979-985.

Vernon, R.H., Johnson, S.E., Melis, E.A., 2004. Emplacement-related microstructures in the margin of a deformed tonalite pluton: the San José pluton, Baja California, México. Journal of Structural Geology 26, 1867-1884.

Vernon, R.H., Williams, V.A., D'Arcy, W.F., 1983. Grainsize reduction and foliation development in a deformed granitoid batholith. Tectonophysics 92, 123-145.

Waldron, H.M., Sandiford, M., 1988. Deformation volume and cleavage development in metasedimentary rocks from the Ballarat slate belt. Journal of Structural Geology 10, 53-62.

White, S.H., 1979. Grain and sub-grain size variation across a mylonite zone. Contributions to Mineralogy and Petrology, 70, 193-202.

White, S. H., Burrows, S. E., Carreras, J., Shaw, N. D. & Humphreys, F. J. 1980: On mylonites in ductile shear zones. Journal of Structural Geology, 2, 175-187.

Wintsch, R.P., Christoffersen, R., Kronenberg, A. K., 1995. Fluid-rock reaction weakening of fault zones. Journal of Geophysical Research 100, 13021-13032.

Wintsch, R.P., Yi, K., 2002. Dissolution and replacement creep: a significant deformation mechanism in mid-crustal rocks. Journal of Structural Geology 24, 1179-1193.

Wintsch, R.P., Aleinikoff, J.N., Yi, K., 2005. Foliation development and reaction softening by dissolution and precipitation in the transformation of granodiorite to orthogneiss, Glastonbury complex, Connecticut, U.S.A. Canadian Mineralogist, 43, 327-347.

Yang, X. Y., O'Hara, K. D. & Moecher, D. P., 1998. Distinction between tectonic mixing and mass transfer processes in a ductile shear zone. Journal of Structural Geology, 20, 1089-1103.

Yonkee, W. A., Parry, W. T. & Bruhn, R. L., 2003. Relations between progressive deformation and fluid-rock interaction during shear-zone growth in a basement cored thrust sheet, Sevier orogenic belt, Utah. American Journal of Science, 303, 1-59.